Discovery of macrocyclic inhibitors of Apurinic/apyrimidinic endonuclease 1

Richard Trilles[¥], Dmitri Beglov[†], Qiujia Chen[§], Hongzhen He[§], Randall Wireman[ǂ], April Reed[ǂ], Spandan Chennamadhavuni[¥], James S. Panek, Lauren E. Brown[¥], Sandor Vajda[†], John A. Porco, Jr.[¥], Mark R. Kelley*[ǂ], and Millie M. Georgiadis*[§⊥]

[¥]*Department of Chemistry and Center for Molecular Discovery (BU-CMD),Boston University, Boston, Massachusetts, 02215,* [†]*Department of Biomedical Engineering, Boston University, Boston, Massachusetts, 02215* [§]*Department of Biochemistry and Molecular Biology,* [ǂ]*Department of Pediatrics and Herman B Wells Center for Pediatric Research, Indiana University School of Medicine, 46202* [⊥]*Department of Chemistry and Chemical Biology, Purdue School of Science, Indiana University-Purdue University Indianapolis, Indianapolis, Indiana 46202*

This is the author's manuscript of the article published in final edited form as:

Trilles, R., Beglov, D., Chen, Q., He, H., Wireman, R., Reed, A., … Georgiadis, M. M. (2019). Discovery of macrocyclic inhibitors of Apurinic/apyrimidinic endonuclease 1. Journal of Medicinal Chemistry. https://doi.org/10.1021/acs.jmedchem.8b01529

Abstract

Apurinic/apyrimidinic endonuclease 1 (APE1) is an essential base excision repair enzyme that is upregulated in a number of cancers, contributes to resistance of tumors treated with DNA-alkylating or -oxidizing agents, and has recently been identified as an important therapeutic target. In this work, we identified *hot spots* for binding of small organic molecules experimentally in high resolution crystal structures of APE1 and computationally through the use of FTMAP analysis (http://ftmap.bu.edu/). Guided by these *hot spots*, a library of drug-like macrocycles was docked and then screened for inhibition of APE1 endonuclease activity. In an iterative process, *hot spot*-guided docking, characterization of inhibition of APE1 endonuclease, and cytotoxicity of cancer cells were used to design next generation macrocycles. To assess target selectivity in cells, selected macrocycles were analyzed for modulation of DNA damage. Taken together, our studies suggest that macrocycles represent a promising class of compounds for the inhibition of APE1 in cancer cells.

Introduction

Targeting of DNA repair proteins for cancer therapeutic development represents a recent area of interest in drug discovery (reviewed in [1]). It has long been known that DNA repair proteins including apurinic/apyrimidinic endonuclease 1 (APE1) are upregulated in cancer and can mediate resistance to a number of chemotherapeutic agents including those that target DNA directly through alkylation or indirectly by mechanisms such as the creation of reactive oxygen species that react with DNA.[2-5] In its essential role in base excision repair (BER), APE1 catalyzes the Mg^{2+}-dependent cleavage of the phosphodiester backbone 5′ of abasic sites that result from removal of damaged bases by glycosylases (reviewed in [6]).

To date, a number of experimental and *in silico* high-throughput screens (HTS) to identify selective APE1 endonuclease inhibitors have been reported.[7-13] These efforts have largely focused on the screening of commercially available libraries of small molecules that would be predicted to bind directly to APE1. In an alternative approach, macrocycles, unrelated to those reported here, have been identified that bind directly to an abasic site in duplex DNA preventing APE1 from binding its substrate.[14] While a number of APE1-targeting compounds exhibit low micromolar activity, demonstrating selectivity has been challenging.[15] Many of the existing inhibitors are negatively charged and disrupt other protein-DNA interactions as well as APE1-DNA interactions. Others, such as antimony-containing compounds, are not cell permeable.[8] Reactive blue 2 dye or myricetin, which inhibit APE1, are also known to bind several cellular targets and are problematic in terms of chemical optimization. Most recently, a novel class of heterocyclic APE1 inhibitors with low micromolar IC_{50}s resulting from a focused medicinal chemistry effort was reported.[16] Existing ligands provide important information about the chemical structure and composition of APE1 endonuclease inhibitors. However, a limitation in the rational design and development of selective APE1 inhibitors remains a lack of structural information for APE1-inhibitor complexes. In this study, we used X-ray crystallography and computational solvent mapping to identify *hot spots* for binding of small organic molecules to APE1. Docking based on consideration of hot spot positioning suggested that macrocycles could bind to the active site of APE1.

Among New Chemical Entities (NCE's) approved as drugs during the period 1981-2006, 60% are natural products and their derivatives.[17] Evolutionarily-driven biosynthesis differs from laboratory organic synthesis, leading to a difference in properties between natural and synthetic compounds.[18] Natural products often violate the molecular weight limit of less than 500 Daltons set by Lipinski's Rule of Five,[19, 20] while remaining pharmacologically active. Many of these violators are macrocycles; it has been observed that macrocycles have an advantage over similarly sized acyclic compounds in terms of pharmacokinetics, solubility, cell permeability, and potency.[21-24] These advantages have been attributed to features such as a diminished entropic penalty on binding, as well as the potential for the dynamic, environmentally-driven alteration of physiochemical properties (*e.g.* intramolecular hydrogen bond-mediated burial of solubilizing polar groups allowing for the traversal of nonpolar membrane environments).[21-23, 25] The main appeal of macrocycles as scaffolds for APE1 ligands is in their ability to provide a semi-flexible, soluble scaffold linking the structural elements able to interact with the distant binding hot spots on the DNA-binding protein surface. Advances in the synthesis of non-natural macrocycles and their extensive testing in drug discovery[26] contributed to the creation of macrocyclic libraries, which are available both academically and commercially.

In a novel approach, *in silico* modeling, guided by our solvent bound APE1 X-ray crystal structures as well as computationally docked solvents that defined "hot spots" for binding of organic molecules, suggested that our macrocyclic libraries could serve as starting points for the structure-based design of APE1 ligands. Accordingly, a library of macrocycles was tested for inhibition of APE1 endonuclease activity, and four novel macrocycles with IC_{50} values in the low micromolar range were identified. Building on these hits, additional macrocycles were synthesized to establish initial structure activity relationship (SAR) contributing to the APE1 inhibitory properties of this newly identified chemotype.

Results and Discussion

Crystallographic solvent mapping for APE1

With a large number of inhibitors reported for APE1, we sought to provide a structural framework for understanding the nature of the interactions. While the inhibitor complex structures have proven elusive, the solvent used to solubilize the inhibitors, DMSO, was bound to the active site of APE1 in numerous structures. We therefore prepared DMSO soaks and obtained a crystal structure of a DMSO-APE1 (PDB ID: 6MK3) complex determined at 1.48 Å (Table 1). In this structure, DMSO binds to two distinct sites within APE1. We refer to the first location within the active site created through interactions with W280, F266, L282, and N174 as the "abasic site or AP (apurinic/apyrimidinic) site" (Figure 1A, B). The sulfoxide O atom of DMSO is hydrogen bonded to the side chain NH of N174 (N-O distance is 2.7 Å) (Figure 1B). N174 is positioned through hydrogen-bonding of its side chain carbonyl to the main chain amide nitrogen of G176 in the repair active site. DMSO bound in the abasic site superimposes directly on the baseless sugar, which is flipped out into a shallow pocket in the structure of the substrate APE1-DNA complex (Figure 1C).[27] The second DMSO binding site is located 35 Å away from the abasic site and involves interactions with D163, F162, L140, and Q137. In this site, the sulfoxide O atom is located 2.7 Å from the main chain N in D163 (Figure S1). This second binding site is an isolated small binding pocket on the surface of the protein.

Table 1: Crystallographic Data

Dataset	**DMSO**	**DMSO/ Mg^{2+}**	**DMSO/ Tris**	**GLC**
PDB ID	6MK3	6MKK	6MKM	6MKO
Data				
a (Å)	46.583	46.697	46.552	46.492
b (Å)	137.789	141.487	136.601	137.815
c (Å)	45.243	45.334	45.084	45.193

Space group	$P2_12_12$	$P2_12_12$	$P2_12_12$	$P2_12_12$
Resolution limit (Å)	1.48	1.44	1.67	2.09
Completeness (%)	97.6 (97.2)	98.4 (74.3)	95.3 (79.4)	99.0 (97.5)
Rmerge (%)	6.0 (41.0)	4.7 (34.0)	7.7 (63.9)	7.7 (21.2)
I/σ	22.8 (3.0)	31.3 (3.4)	16.5 (2.1)	30.4 (4.2)
Refinement				
R value (%)	19.1	18.4	20.5	17.6
R free (%)	21.9	21.2	25.0	22.8
RMSD bonds (Å)	0.005	0.007	0.004	0.003
RMSD angles (°)	1.03	1.177	0.934	0.810
Average B-factor	20.2	18.4	24.1	21.3

Highest resolution shells in order of appearance in table: 1.51-1.48, 1.46-1.44, 1.7-1.67, 2.12-2.09.

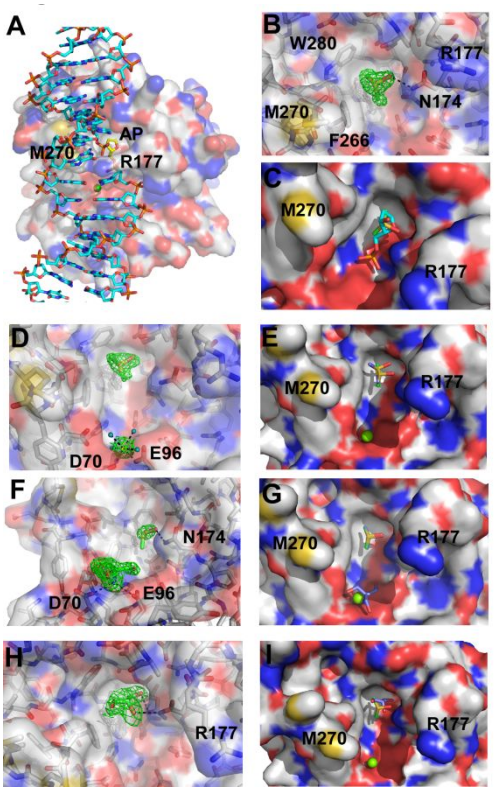

Figure 1. Crystallographic solvent mapping. (A) A molecular surface rendering of APE1, the DMSO bound structure (6MK3), with C, light gray, O, red, N, blue, and S, yellow. Superimposed on the molecular surface of APE1 is DNA (from 4IEM) in a stick rendering, C, cyan, P, orange, O, red, and N, blue with the abasic or AP residue in yellow. (B) DMSO bound to the abasic site of APE1. The initial Fo-Fc electron density map contoured at 3σ is shown for the crystal structure with DMSO bound to the AP site. A hydrogen bond between the O of DMSO and NH of N174 is indicated by a black dashed line. APE1 is shown as a semi-transparent molecular surface rendering. Residues W280, F266, L282 (not labeled, directly underneath the bound DMSO), and N174 line the shallow AP site pocket. (C) DMSO (C, green, S, yellow, O, red) is shown superimposed with the abasic substrate (C, cyan) in stick renderings. (D) DMSO and Mg^{2+} bound to the active site of APE1. The initial Fo-Fc electron density map of the DMSO/Mg^{2+} crystal structure (6MKK) is shown for DMSO and Mg^{2+} contoured at 3σ. Coordinating ligands for Mg^{2+} are shown in dashed black lines including D70, E96, and 4 water molecules. The DMSO is this structure is not hydrogen bonded to N174. (E) DMSO and DMSO/Mg^{2+} are shown superimposed in

the abasic site pocket on a surface rendering of APE1. In the presence of Mg^{2+}, the DMSO (C, blue) position is slightly shifted relative to that in the structure with just DMSO (C, green) bound. (F) Tris and DMSO bound to the active site of APE1 (6MKM). The initial Fo-Fc electron density map for Tris and DMSO is shown contoured at 3σ. Tris is hydrogen bonded to D70 and E96, the Mg^{2+} coordinating ligands. (G) Tris/DMSO are shown in stick renderings superimposed on the DMSO bound structure. Mg^{2+} from the DMSO/Mg2+ structure is shown for reference. Tris binds to the Mg^{2+} site. DMSO binds very similarly in the two structures. (H) Glycerol bound to the active site of APE1 (6MKO). The initial Fo-Fc electron density map is shown contoured at 3σ. Hydrogen bonds between OH group in glycerol and NH in N174 and N212 are shown in dashed black lines. (I) Glycerol (C, blue) is shown superimposed with DMSO and Mg^{2+} from the DMSO/Mg^{2+} structure for reference. Glycerol binds deeper in the abasic site pocket than DMSO.

Additional complexes with DMSO include a DMSO/Mg^{2+} complex (PDB ID: 6MKK) and a DMSO/Tris complex (PDB ID: 6MKM). These complexes were obtained by screening for APE1-small molecule complexes, the first with 4-(hydroxymethyl)-phenyl-acetic acid, a compound selected for its potential to bind to the abasic site and to Mg^{2+} in the active site, and the second with an arylstibonic acid derivative, the APE1 inhibitor 13755,[8] soaked in Tris pH 8.0 (See Materials and Methods). Neither 4-(hydroxymethyl)-phenyl-acetic acid nor 13755 were evident in the electron density maps for these crystals. However, these structures, determined at 1.44 and 1.67 Å, respectively, provided additional insights on DMSO binding in the presence of other bound ligands in the active site, as Mg^{2+} and Tris in these structures are bound to the same site. Mg^{2+} exhibits an octahedral coordination geometry with oxygen atoms from D70 and E96, each 2.1 Å from the Mg^{2+} atom, serving as ligands as well as four water molecules (Figure 1D). DMSO is bound deeper within the abasic site pocket and is not hydrogen bonded to N174 (Figure 1E); its sulfoxide oxygen now faces the backbone carbonyl of A230. The NH_3^+ group of Tris is hydrogen bonded to the O of D70 (2.7 Å) and to O of E96 (3.2 Å) (Figure 1F). DMSO binds slightly differently in the presence of bound Mg^{2+} than in the presence of Tris. In the DMSO/Tris

structure and DMSO only structures, DMSO is bound identically in the abasic site (Figure 1G). The second DMSO site is also identically occupied in these two structures, whereas in the DMSO/Mg^{2+} structure, the second DMSO site is not occupied. This finding suggests that the presence of Mg^{2+} modulates positioning and availability of small molecule binding sites in APE1.

Additional solvents that bind to the abasic sugar binding site within the repair active site of APE1 include glycerol (PDB ID: 6MKO) and ethylene glycol. The basis for solvent binding within the repair active site of APE1 appears to rely on an interaction with the relatively small pocket designed to bind to the flipped out abasic sugar of substrate DNA. Binding of glycerol to the abasic site involves a hydrogen bonding interaction between a hydroxyl group in glycerol and the side chain carbonyl oxygen of N212 (2.79 Å) and a water-mediated hydrogen-bonding interaction between a second glycerol hydroxyl and the amide side chain group of N174 (Figure 1H). The more polar glycerol binds a little deeper in the pocket than DMSO alone (Figure 1I). The second glycerol binding site is located between two molecules in the lattice and forms a hydrogen bond between one of its hydroxyl groups and the main chain carbonyl oxygen of E242 (3.08 Å) (Figure S1). Ethylene glycol was used as the cryoprotectant in all structures except for that of the glycerol structure. Hydrogen bonding occurs between the carboxylate oxygen atom of E216 and a hydroxyl of ethylene glycol bound to APE1 in all of the structures in which ethylene glycol was used as a cryoprotectant (Figure S1). Three additional ethylene glycol binding sites were identified in the DMSO structure and two additional sites in the previously reported Apo structure,[28] including one bound to the abasic site (Figure S1).

Computational solvent mapping

The crystallographic solvent mapping results provided a relatively small number of preferred binding sites within APE1. Therefore, it was of interest to use computational methods to further investigate possible binding sites. Results of computational solvent mapping for the magnesium-bound APE1 structure are shown in Figure 2. The primary binding region (Figure 2A) is composed of 7 consensus sites with the total population of 50 probe clusters. The most populated site, site 1 (17 probe

clusters) is next to the magnesium ion position (shown in green). Site 2 (15 clusters) is the abasic DNA sugar binding site. We have experimentally validated binding of Tris near the Mg^{2+} site in the Tris/Mg^{2+} structure and binding to the abasic site by solvent probes such as DMSO, ethylene glycol, and glycerol as determined by multiple solvent crystal structures. The computational mapping also revealed a binding region consisting of a small hydrophobic cavity on the opposite side of the protein, formed by Leu 62, Ile 91, Phe 162, Phe 165, and Leu 318 residues. Two clusters with a total of 21 probes are located in this region (Figure 2B). The crystallographic experiments showed an ethylene glycol bound at this secondary region. Collectively, our crystallographic and computational solvent mapping provided the locations of preferred binding sites for small organic molecules in the active site of APE1 in the presence and absence of the APE1 cofactor, Mg^{2+}, laying the foundation for a novel structure-based approach for the identification of APE1 inhibitors.

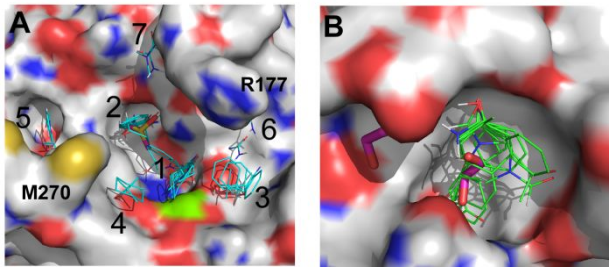

Figure 2. Computational solvent mapping with FTmap ((http://ftmap.bu.edu/). (A) Computational docking of small organic molecules reveals clustering of 50 probes (thin lines, C, cyan, O, red, N blue) into 7 consensus sites in or near the active site of APE1 (4QHE) shown as a molecular surface rendering (C, light gray, O, red, N, blue, and S, yellow). DMSO (stick model C, green, O, red, S, yellow) from the crystal structure is shown bound in consensus site 2. Probes at consensus site 1, the most populated site, are in close proximity to the Mg^{2+} ion, shown as a surface rendering in green. (B) A secondary site occupied by ethylene glycol in several crystal structures of APE1 is shown with a cluster of 21 probes shown in thin lines. Ethylene glycols bound in this site and in the vicinity are shown as stick renderings (C, magenta, O, red). This is a small pocket on the surface of the molecule. Thus, the major consensus sites for computational docking of probes in the active of APE1 and in another pocket have been validated in our crystallographic analysis.

Identification of macrocycles that inhibit APE1 endonuclease activity

Focusing on sites 1 and 2 as a key binding regions for potential APE1 inhibitors, we deduced that sites 3-7 show directions of possible ligand extensions. The distance between clusters 5 and 6 spanning the binding pocket is approximately 18 Å, suggesting that an optimal ligand for this binding region may be large in size. This observation of a large pocket size led us to consider the *in silico* evaluation of a small library of 15- and 16-membered macrocycles (105 compounds) from the BU-CMD screening collection as potential inhibitors (**MC001-MC105**, see Scheme 1 for general synthetic route). These macrocycles possess molecular weights ranging from 350-800 kDa and maximal projection radii ranging from 6-10 Å. The library was originally synthesized according to the protocol outlined in Scheme 1.

Specifically, enantioenriched homoallylic amines **5** were first prepared *via* asymmetric crotylation of imine carbamate substrates with enantioenriched crotylsilane **2**. These acyl imines were generated *in situ* by condensation of allyl carbamate **1** with a variety of aldehydes **3a-e** in a modified variant of our previously-reported procedure.[29] While Scheme 1 depicts the stereochemical outcome achieved from the use of (*S*)-**2**, the screening library was also populated with macrocycles derived from the enantiomeric crotylsilane (*R*)-**2**, leading to macrocycles, which are epimeric at the crotylation-derived stereocenters.[30] Subsequent palladium-mediated allyl carbamate deprotection of **4** afforded homallylic amines **5**, which were then further diversified *via* EDCI-mediated coupling to various commercial, Boc-protected amino acids **6a-d** to afford **7**. Following deprotection of **7**, macrocycles **MC001**-**MC105** were obtained *via* a tin-mediated tandem, one-pot aminolysis/macrolactonization of amino esters **8** with various γ-butyro or δ-valero lactone derivatives **9a-s.**[31]

Scheme 1: General design and synthetic route for macrocyclic lactone library.[i,ii]

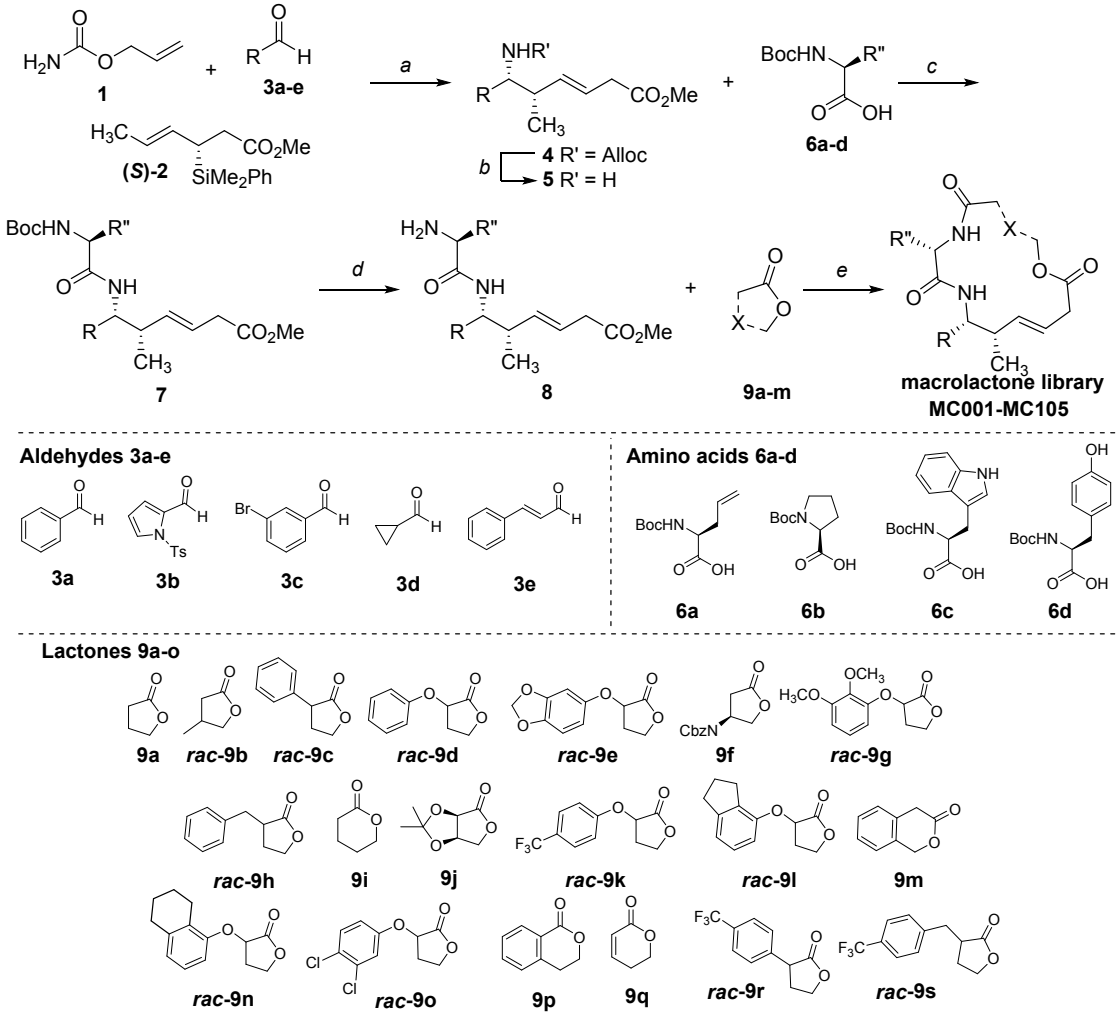

[i]Reagents and conditions: (a) BF_3-THF, -78 °C to -20 °C; (b) $Pd(PPh_3)_4$, 1,3-dimethylbarbituric acid, THF; (c) EDCI, *i*-Pr_2EtNH, DMF or CH_2Cl_2; (d) HCl, dioxane; (e) Otera's catalyst, $PhCF_3$

[ii] Depicted stereochemistry corresponds to use of (*S*)-2 in Step a. Intermediates **4**, **5**, **7**, **9**, and macrocycles **MC** derived from crotylsilane (*R*)-2 are epimeric at the methyl- and R-substituted positions.

We computationally docked this macrocyclic library, guided by hot spots identified by our crystallographic solvent mapping and FTMap analysis as described in Experimental Procedures. Docking yielded a series of high quality poses, suggesting that select BU-CMD macrocycles generally match the topological features of the APE1 binding site. The docked molecules were scored on the basis of the average ensemble energy for their lower energy poses as described in the Experimental Procedures. The top 25 docked molecules and their average ensemble energies are shown in Table 2. Notably, macrocycles derived from (*S*)-**2** and tryptophan (**6c**) predominated among the top scored macrocycles.

Table 2. Average Autodock energy for the top 25 macrocycles

Code	Crotylsilane	Aldehyde **3**	Amino acid **6**	Lactone **9**	Energy
MC042 (α-*R*)	(*S*)-**2**	**3b**	**6c**	(*R*)-**9c**	-9.38
MC093 (α-*S*)	(*R*)-**2**	**3e**	**6c**	(*S*)-**9d**	-9.19
MC048	(*S*)-**2**	**3b**	**6c**	**9p**	-9.18
MC044	(*S*)-**2**	**3b**	**6c**	**9f**	-9.08
MC042 (α-*S*)	(*S*)-**2**	**3b**	**6c**	(*S*)-**9c**	-9.02
MC047 (α-*S*)	(*S*)-**2**	**3b**	**6c**	(*S*)-**9k**	-8.95
MC043 (α-*S*)	(*S*)-**2**	**3b**	**6c**	(*S*)-**9d**	-8.91
MC046	(*S*)-**2**	**3b**	**6c**	**9j**	-8.87
MC030 (α-*S*)	(*S*)-**2**	**3a**	**6c**	(*S*)-**9l**	-8.77
MC022 (α-*R*)	(*S*)-**2**	**3a**	**6c**	(*R*)-**9h**	-8.76
MC047 (α-*R*)	(*S*)-**2**	**3b**	**6c**	(*R*)-**9k**	-8.63
MC022 (α-*S*)	(S)-**2**	**3a**	**6c**	(*S*)-**9h**	-8.63
MC045	(*S*)-**2**	**3b**	**6c**	**9i**	-8.58
MC093 (α-*R*)	(*R*)-**2**	**3e**	**6c**	(*R*)-**9d**	-8.58
MC032 (α-*R*)	(*S*)-**2**	**3a**	**6c**	(*R*)-**9n**	-8.55
MC043 (α-*R*)	(*S*)-**2**	**3b**	**6c**	(*R*)-**9d**	-8.50

MC030 (α-*R*)	(*S*)-**2**	**3a**	**6c**	(*R*)-**9l**	-8.49
MC019 (α-*R*)	(*S*)-**2**	**3a**	**6c**	(*R*)-**9e**	-8.48
MC061	(*R*)-**2**	**3c**	**6c**	**9m**	-8.47
MC096	(*R*)-**2**	**3e**	**6c**	**9m**	-8.45
MC033 (α-*S*)	(*S*)-**2**	**3a**	**6c**	(*S*)-**9o**	-8.45
MC036 (α-*R*)	(*S*)-**2**	**3a**	**6c**	(*R*)-**9s**	-8.45
MC019 (α-*S*)	(*S*)-**2**	**3a**	**6c**	(*S*)-**9e**	-8.45
MC058 (α-*R*)	(*R*)-**2**	**3c**	**6c**	(*R*)-**9d**	-8.44
MC058 (α-*S*)	(*R*)-**2**	**3c**	**6c**	(*S*)-**9d**	-8.44

Based on favorable preliminary docking results, macrocycles available at the time of screening were then assayed as potential inhibitors of APE1 activity. Of the 66 compounds assayed, four (see below for codes) inhibited APE1 endonuclease activity by at least 45% and were further characterized for concentration dependent inhibition. Using this approach, 6.1% of the compounds screened were found to inhibit APE1, whereas in our previous HTS efforts, the success rate was approximately 0.1%.[10] All four of the compounds, **MC043, MC047, MC042 and MC019** exhibited concentration dependent inhibition with IC_{50} values ranging from 1.2 μM to 5.4 μM for the diastereomeric mixtures (Figure 3).

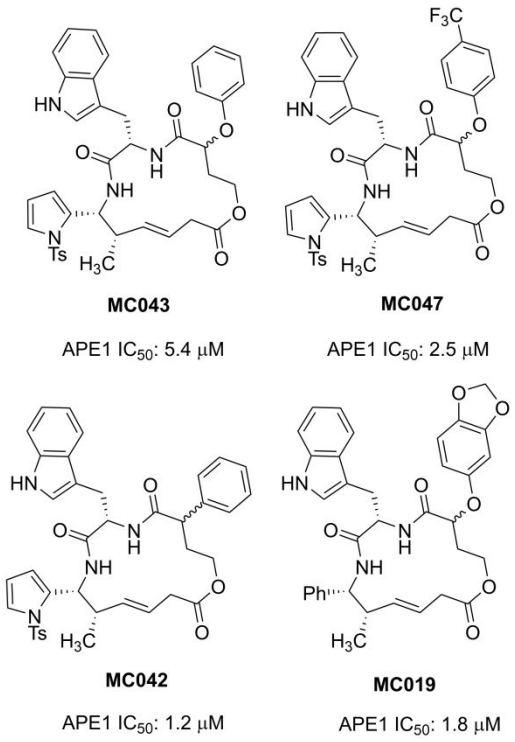

Figure 3. Initial hits from high-throughput screen of the macrocycle library. The chemical structures of the four hits obtained from screening of 66 macrocycles in an *in vitro* endonuclease activity are shown along with the IC50 values.

From the primary screen, nascent SAR emerged suggesting that APE1 endonuclease inhibition activity was confined to library members originating from crotylation of *N*-tosyl pyrrole 2-carboxaldehyde (**3b**) or benzaldehyde (**3a**) with crotylsilane (*S*)-**2**, and Boc-*L*-tryptophan (**6c**) as the amino acid building block (Scheme 1). These results were highly consistent with the outcome of our docking studies, in which these modalities appeared frequently among the top 25 structures. In addition, both diastereomers of all active hits are represented in the top 25 structures (Table 2).

With active macrocycles in hand, we next revisited our docking results to identify consensus poses for the actives that might inform further docking studies and analog designs. In general, two distinct docking modes with comparable energies were observed for the active macrocycles. Figure 4 depicts low-energy poses representing the two alternative binding modes of active macrocycle **MC047** as an

illustrative example. **MC047**, which was screened as a mixture of diastereomers, was docked separately as the α-*S* (green) and α-*R* (cyan) diastereomers, which refers to stereochemistry at the position α- to the macrolactone carbonyl. The docking poses of Mode 1, shown in Figure 4A, occupy 6 out of 7 hot spots in the main binding site. The difference in binding for the two diastereomers is mainly due to a slight change in the positioning of the tryptophan indole as depicted in Figure 4A. Specifically, this heterocycle is parallel to the plane of the Met270 hydrophobic atoms in the pose for the α-*S* isomer, while the pose for the α-*R* isomer projects the indole N-H toward this plane. It is interesting to observe that bound DNA (PDB ID: 1DE9) shares a bicyclic heterocycle positioned below Met270, similar to the Mode 1 docking pose. (Figure 4B hotspot region 4). The main feature of binding Mode 2, in contrast, is an interaction of the sulfonamide group with the magnesium ion, as shown in Figure 4C. This pose, which was only obtained for the *N*-tosylpyrrole-containing macrocycles, occupies 5 out of 7 hot spots in the main binding site. For **MC047**, the trifluoromethyl group of the α-*S* isomer extends toward an additional hot spot (number 5 in Figure 2A), while in the α-*R* pose this group interacts with the terminal carbon of Met270. In comparing this Mode 2 pose to the binding mode of DNA, the lactone oxygens are situated proximal to where the DNA phosphate group binds the Mg^{+2} ion (Figure 4 D, hotspot region 2).

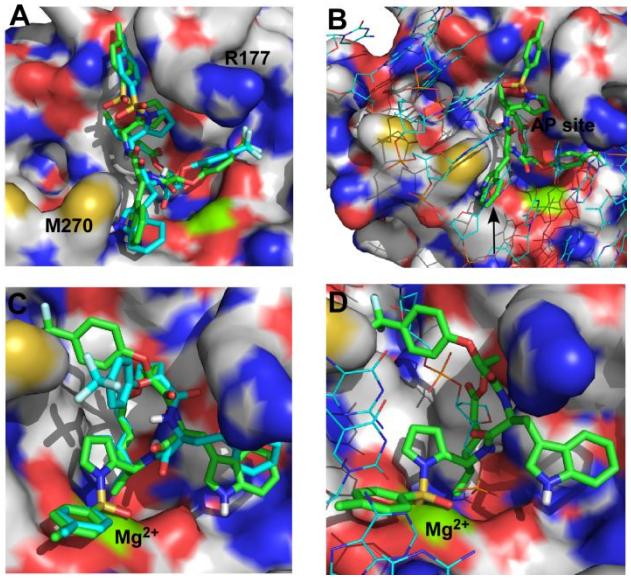

Figure 4. Docking of macrocycle hit **MC047**. (A) The two diastereomers of **MC047** are shown as stick models with α-*S* (C, green) and α-*R* (C, cyan) for Mode 1 of the possible docking poses. APE1 (4QHE) is shown as a molecular surface rendering. In docking Mode 1, **MC047** diastereomers occupy 6 out of 7 hot spots in the main binding site. The difference in binding for the two diastereomers is mainly due to a slight change in positioning of the tryptophan indole. The orientation is similar to that shown in Figs. 1 and 2 as can be seen by the relative positions of M270 and R177. (B) In binding Mode 1, the position of the bicyclic heterocycle of **MC047** (C, green) coincides with that of a guanine nucleotide from DNA (thin lines, C, cyan) bound to APE1 (1DE9) superimposed on the apo APE1 structure. APE1 is shown as a molecular surface rendering. (C) The two diastereomers of **MC04**7 are shown in Mode 2 as similar renderings to those in (A), α-*S* (C, green) and α-*R* (C, cyan). In this binding mode, the sulfonamide group is in close proximity to the Mg^{2+} ion (green on the molecular surface rendering). The Mode 2 pose was only obtained for the *N*-tosylpyrrole-containing macrocycles and occupies 5 out of 7 hot spots in the main binding site. For **MC047**, the trifluoromethyl group of the α-*S* isomer extends toward an additional hot spot (number 5 in Figure 2A), while in the α-*R* pose this group interacts with the terminal carbon of Met270. (D) **MC047** α-*S* (C, green) is shown with superimposed DNA (1DE9). In this mode, the lactone oxygens are situated proximal to where the DNA phosphate group binds the Mg^{2+} ion near hotspot region 2).

Synthesis and *in vitro* assessment of follow-on analogs

As part of our initial validation of the chemotype, a small set of simplified analogs **10**-**13** were synthesized (Scheme 2). APE1 endonuclease activities for these lactones are shown in Table 3. Among this set, the *N*-tosyl pyrrole-substituted analogs **12** and **13** displayed superior APE1 inhibition potencies for the macrocycles in comparison to their phenyl-substituted counterparts **10** and **11**. Interestingly, the most potent macrolactone of this set, compound **13**, also falls in the top 25 docked macrocycles from the virtual library (**MC045**, Table 2) These observations led us to focus on binding Mode 2 (*cf.* Figures 4C and D), which exhibits a key interaction between the sulfonamide and Mg^{2+} ion, for subsequent docking experiments. Following identification of the initial screening hits and simplified analogs, our subsequent

optimization efforts focused on exploring further modifications of the linker group connecting the *L*-tryptophan/homoallylic amine core, with the parallel goals of improving both potency and drug-like properties of the chemotype. A liability of lactone- and ester-containing drugs (as exemplified in macrocyclic lactone drugs with bacterial resistance mechanisms toward macrolide antibiotics) is the potential for drug inactivation due to esterase-mediated hydrolysis.[32, 33] To address this anticipated liability, we next targeted macrolactam analogs (Scheme 3). Substrates **7a** and **7b** were deprotected and coupled to various achiral unsubstituted (**14a**-**14c**) and chiral, nonracemic (**14d**-**14k**) Boc-protected β-, γ- and δ-amino acids (Scheme 3 and Table 4). Following coupling, tandem Boc- and methyl ester deprotections were followed by HATU-mediated macrolactamization to afford macrocyclic lactams in modest yields for the three-step sequence in most cases (Table 4).

Scheme 2: Synthesis of simplified follow-on macrolactone analogs.

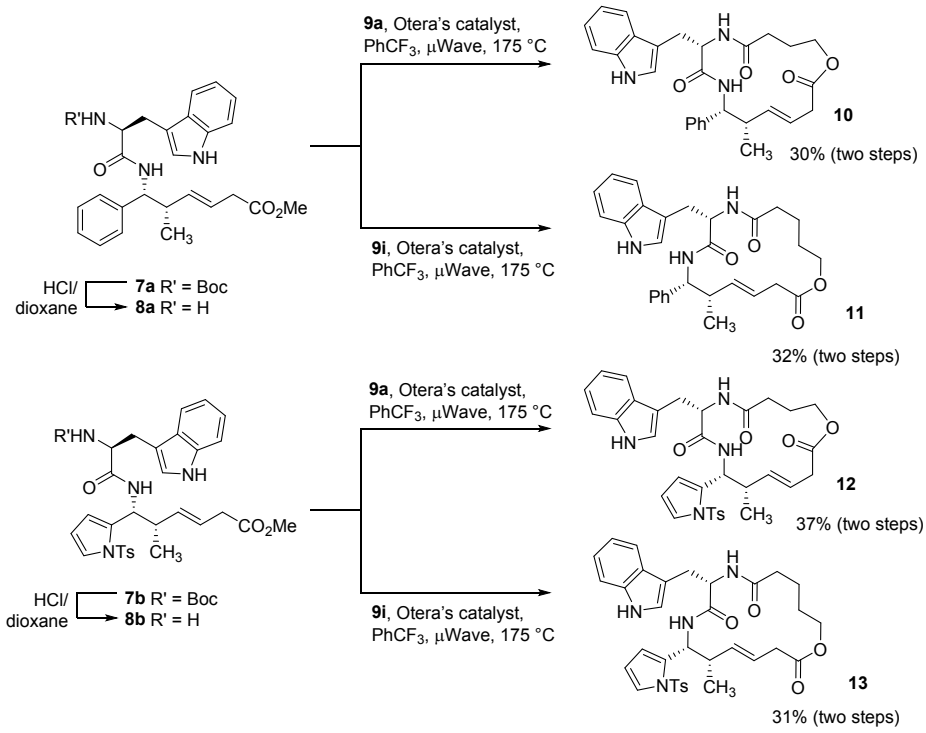

Table 3. APE1 endonuclease activity of macrolactones **10**-**13**

Entry	Compound	APE1 IC_{50} (μM)	PaO2c EC_{50}(μM)
1	**10**	>100	>100
2	**11**	63.5	>50
3	**12**	10.6	>100
4	**13**	9.3	>100

The structures and APE1 endonuclease activities of macrocycles **17**-**30** are shown in Table 4. Initially, the direct *O*- to *N*- replacement was probed using compounds **17** and **18**, the direct lactam analogs of lactones **12** and **13**, respectively, as well as the 14-membered macrolactam **19** derived from β-alanine. A drop in activity was observed for all unsubstituted compounds **17**, **18**, and **19**. For follow-on substituted lactam analogs, a cohort of chiral amino acids **14d-k** were selected based on additional

docking experiments. Specifically, a large virtual library comprised of lactams derived from commercially-available amino acid building blocks was docked and evaluated, and the macrocyclic lactams that produced the lowest energy poses in binding Modes 1 and 2 were selected for synthesis and evaluation. In addition to the tosyl pyrrole-substituted macrolactams **17**-**27**, phenyl-substituted variants of select analogs (**28**-**30**) were also synthesized for comparison.

Scheme 3: General synthetic route toward second-generation macrocyclic lactams.[i]

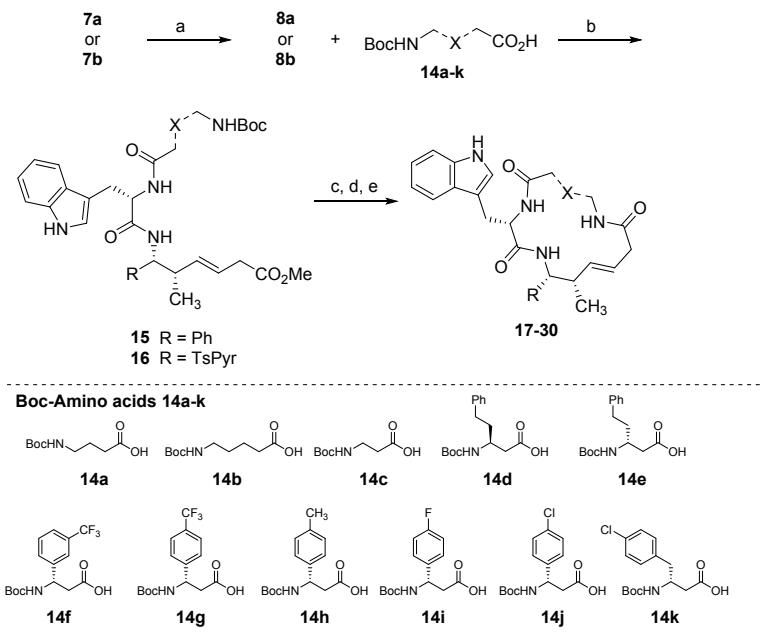

[i]Reagents and Conditions: (a) HCl/dioxane; (b) HATU, *i*-Pr_2EtNH, CH_2Cl_2; (c) 2.5M NaOH, THF; (d) HCl, dioxane; (e) HATU, *i*-Pr_2EtNH, CH_2Cl_2

Similar to the macrolactone series, there appear to be key substitution patterns on the tethering β-amino acid of the 14-membered macrolactam scaffolds that govern endonuclease activity. For example, substitution α- to the lactam carbonyl appears to impart enhanced potency in most cases, while the comparison of lactams **20** and **21** suggests that this position may not be sensitive to stereochemical inversion. This result is generally consistent with our docking, wherein both epimers generally produced favorable docking poses. Much like the lactone series, the *N*-tosyl pyrrole-substituted lactams **23**, **25**, and

26 also all exhibited superior potencies to their phenyl-substituted counterparts **28**, **29** and **30**, respectively. Interestingly, the *meta*-(trifluoromethyl)phenyl macrolactam **22** exhibited a significant reduction in activity in comparison to its *para*-substituted phenyl and benzyl analogs **23-27**.

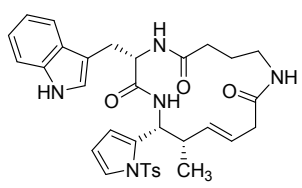

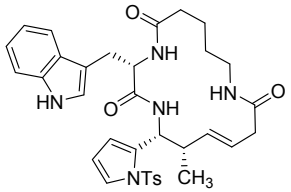

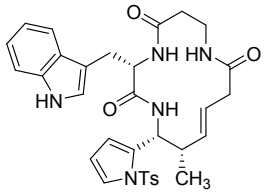

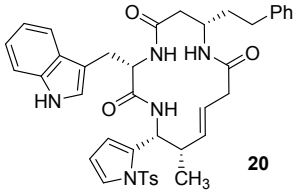

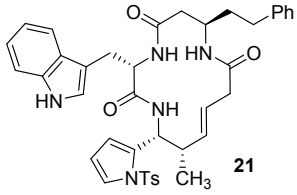

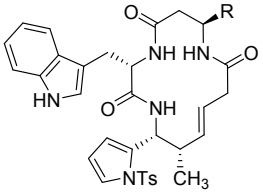

22 R = 3-CF_3Ph
23 R = 4-CF_3Ph
24 R = 4-CH_3Ph
25 R = 4-FPh
26 R = 4-ClPh
27 R = 4-ClBn

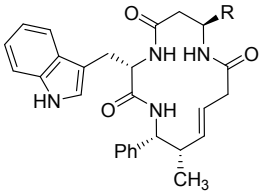

28 R = 4-CF_3Ph
29 R = 4-FPh
30 R = 4-ClPh

Table 4. Synthetic yields and APE1 endonuclease activity of 14-16-membered macrolactams

Entry	Compound	Trp-coupled precursor	Cyclization precursor (yield from **7**)	Cyclization yield (3 steps)	APE1 IC_{50} (μM)	PaO2c EC_{50} (μM)
1	**17**	**7b**	**16a** (81%)	29%	29.2	35.0
2	**18**	**7b**	**16b** (74%)	22%	>50	>100
3	**19**	**7b**	**16c** (93%)	41%	33.2	58.4
5	**20**	**7b**	**16d** (81%)	86%	2.6	>100
6	**21**	**7b**	**16e** (82%)	47%	2.7	>100
7	**22**	**7b**	**16f** (77%)	36%	52.6	6.7
8	**23**	**7b**	**16g** (70%)	46%	1.3	>100

9	**24**	**7b**	**16h** (81%)	32%	2.5	>100
10	**25**	**7b**	**16i** (79%)	42%	5.7	>100
11	**26**	**7b**	**16j** (84%)	43%	12.1	>100
12	**27**	**7b**	**16k** (80%)	42%	1.9	>100
13	**28**	**7a**	**15g** (75%)	25%	26.5	58.5
14	**29**	**7a**	**15i** (77%)	33%	55.1	36.2
15	**30**	**7a**	**15j** (78%)	13%	>100	22

In summary, the observed SAR is generally consistent with the consensus binding Mode 2 observed in our docking studies. Figure 5 depicts an overlay of the consistent low energy Mode 2 binding poses of molecules **MC047**, **11**, **26** and **27**. Molecules **MC047**, **26** and **27** all demonstrate projection of halogen moieties toward the hotspot region 5, as well as the interaction of sulfonamide groups with the magnesium ion. Attempts to validate the computationally-obtained poses through soaking into preformed crystals or co-crystallization experiments employing the most potent APE1 inhibitors have thus far yielded only solvent bound structures as we obtained for other classes of APE1 inhibitors. Notably, the first glycerol-APE1 structure shown in Figure 1 was serendipitously obtained through soaking efforts with macrocycle **20**.

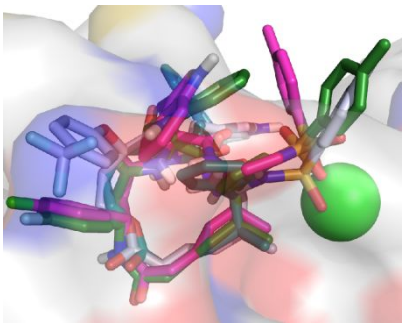

Figure 5. Overlay of "Mode 2" docking poses obtained for stick renderings of **MC047** (C, light gray), **11** (C, teal), **25** (C, dark green) and **26** (C, pink) in the active site of APE1 (4QHE). Compounds **MC047**, **25**

and **26** all display an interaction between the sulfonamide groups and the magnesium ion (light green sphere), as well as a projection of their halogenated aryl rings toward hotspot region 5, left hand side.

Effect of macrocycles on viability and repair of DNA damage in cancer cells

With a series of validated biochemical APE1 inhibitors in hand, we next sought to understand the effects of these inhibitors in a cellular context. Knock-down of APE1 arrests the growth of ovarian cancer cells in a xenograft mouse model;[34] thus, compounds that specifically inhibit APE1 might be expected to have low cytotoxicity in cancer cell culture models. In contrast, compounds that exhibit high cytotoxicity may have off-target effects. Most of the macrocycles tested exhibit low cytotoxicity with the exception of **17**, **19**, **22**, **28**, **29**, and **30** (Tables 1 and 2). However, low cytotoxicity cannot be distinguished from low cell permeability in cell viability assays.

To determine whether the compounds inhibit APE1 endonuclease activity in the cell, DNA damage in cells treated with selected macrocycles was assessed by comet assays[35, 36] done in the presence and absence of the DNA-damaging agent, methyl methanesulfonate, MMS, which alkylates DNA. The comet assay was selected as a cell-based assay that reliably reports single-strand and double-strand breaks in DNA. In this assay, following exposure to MMS, alkylated bases are removed by DNA glycosylases creating abasic sites. APE1 then cleaves the DNA 5′ of the abasic sites leading to single strand breaks (or potentially double-strand breaks if single-strand breaks are produced proximally in both strands). The breaks produce a long tail in the alkaline comet assay analyzed 1 h after adding MMS; this time point is short enough to ensure that the first two steps of base excision repair, removal of the damaged base by a DNA glycosylase and processing by APE1, have occurred. It is, however, insufficient time for the cell to have completed repair of the DNA through the base excision repair pathway. If the macrocycle inhibits APE1 preventing cleavage of the DNA backbone, then the length of the DNA tail in the comet assay is expected to be shorter than that observed for treatment with MMS alone. An inherent assumption for the comet assay is that only compounds that exhibit some level of cell permeability have the potential to affect the tail length of the DNA.

Macrocycles chosen for the alkaline comet assay include non-cytotoxic APE1 inhibitors of varying potency (Tables 3 and 4): **13** (IC_{50} 9.3 μM, EC_{50} > 100 μM), **21** (IC_{50} 2.7 μM, EC_{50} > 100 μM), **23** (IC_{50} 1.3 μM, EC_{50} > 100 μM), and **24** (IC_{50} 2.5 μM, EC_{50} > 100 μM), as well as low-potency APE1 inhibitors with moderate cytotoxicities **19** (IC_{50} 16.9 μM, EC_{50} 58.4 μM) and **28** (IC_{50} 26.5 μM, EC_{50} 58.5 μM). Malignant peripheral nerve sheath tumor ST8814 cells were treated with the macrocycles in the presence and absence of MMS at either 100 μM or, in the case of cytotoxic compounds, the EC_{30} value, and then assessed for comet tail length (Figure 6). The concentrations were selected to deliver the highest possible concentration of macrocycle to the cells without causing significant cell death. Alkaline comet assay results for **19** and **23** are similar to those obtained for MMS alone suggesting that these macrocycles do not effectively inhibit APE1 endonuclease activity in the cell. Macrocycle **28** had a very modest effect on tail length consistent with its modest IC_{50} value for APE1 inhibition. Macrocycles **21** and **24** appear to reduce comet tail length, while macrocycle **13** had the largest impact on tail length. These results suggest that despite having EC_{50} values for cell killing of greater than 100 μM, these compounds appear to permeate cells.

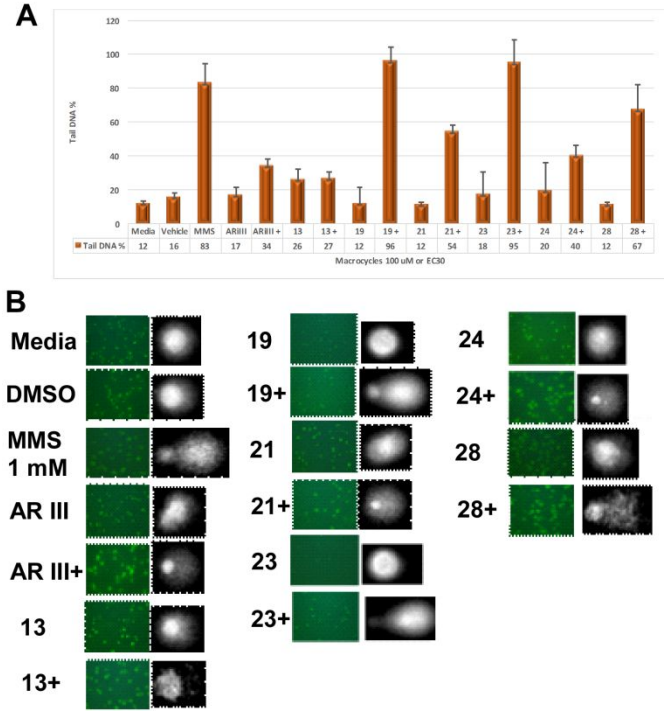

Figure 6. Macrocycle treatment alone and in combination with DNA damaging agent Methyl methanesulfonate (MMS) in Malignant peripheral nerve sheath tumor cell line ST8814 in Alkaline Comet Assay. APE1 Repair inhibitor candidates (Macrocycles) and APE1 Repair inhibitor control, APE1 Repair Inhibitor III (ARiIII; Calbiochem), were tested in ST8814 at a single dose (100 uM; or EC30) and in combination with a single dose of MMS (1.0 mM) for a 1.0 hour treatment. Cells were seeded in 6-well tissue culture plates at 130,000 cells/well in DMEM + 10% FBS and grown overnight at 37 ºC, 5% CO_2. Media was exchanged with Opti-MEM™ (Gibco™) media containing macrocycle alone or spiked with 1.0 mM MMS. Cells were then incubated for 1.0 hour at 37 ºC, 5% CO_2. Media was exchanged with PBS, and cells were treated with 0.25% Trypsin (HyClone™), collected, and washed with PBS. Cells were then counted by hemacytometer. DNA damage was evaluated by CometAssay® (Trevigen®) performed under alkaline conditions. Cells were resuspended in PBS at 1 x 10^5/mL, and then added to pre-melted and cooled (37 °C) agarose at a 1:10 ratio. Cells were gently mixed, and then 50 uL of the agarose cell mix was transferred to pre-warmed comet slides (37 °C; CometSlide™). After solidifying at 4 °C, slides were placed in lysis solution for 60 minutes, and then placed in freshly prepared alkaline unwinding solution (NaOH; pH 13) for 20 minutes. Slides were then subjected to electrophoresis under alkaline conditions (NaOH; pH 13) at 1 Volt/cm (300 mA) for 30 minutes. Slides were washed in H_2O, placed in 70% ethanol, and allowed to dry at 37 ºC for 30 minutes. Slides were stained with 100 µL of 1:10,000 diluted SYBR® Gold (Invitrogen™) in TE pH 7.5, and incubated for 30 minutes. Slides were then rinsed in H_2O briefly, and comets were captured by Fluorescent microscope (Leica DMIL) and quantified by CometScore™ Pro (TriTec Corp®). DNA damage measured by percent Tail DNA for controls and selected macrocycles is shown in (A) in two independent experiments. Representative images of comet slide DNA damage are shown in (B) for controls and selected macrocycles. Average of 20 comet readings/compound.

Conclusion

We have employed a novel computational and structure-based approach to predict and identify new macrocyclic inhibitors of the DNA repair protein APE1. From screening of a library of 66

macrocyclic scaffolds, four compounds were identified with micromolar APE1 inhibition values. The chemotype was further explored and preliminary structure-activity relationships were determined. Our preliminary characterization of the effects of the compounds on cellular activities indicates that at least three of the macrocycles (**13**, **21**, and **24**) are effective in a cellular context (with **13** being the most effective) as assessed by comet analysis following treatment with MMS while retaining reasonable potency for inhibition of endonuclease activity *in vitro*. These results are promising and support further development of these chemotypes as APE1 inhibitors.

Experimental Methods

Preparation of APE1 protein. For crystallization, a single amino-acid substitution (C138A) was introduced within the N-terminally truncated protein lacking the first 40 amino acids (Δ40APE1). DNA encoding residues 40-318 of APE1 was inserted within the PET28A vector by using the NheI and XhoI restriction sites. Site-directed mutagenesis was then used to introduce a C138A mutation and confirmed by DNA sequencing. This protein was expressed as an N-terminal hexa-His tagged protein and purified as previously described for the C65A and wild-type Δ40APE1 proteins.[37] In brief, the cells were lysed by using a French press, and the crude extract was subjected to purification by Ni-NTA and SP-Sepharose ion-exchange chromatography. The affinity tag was then removed by treatment with thrombin, and the protein was further purified by SP-Sepharose ion-exchange chromatography.

Crystallization and data collection. Crystals were obtained by mixing equal parts (1 μl each) of microseeds with a precipitant solution containing 100 mM MES, pH 6.0, 200 mM NaCl and 18-21% PEG4000 and Δ40 hAPE1 C138A (10 mg/ml) buffered in 10 mM HEPES pH 7.5. Self-nucleated crystals of APE1 were obtained under similar conditions and used to produce microseeds.

Solvent-bound complexes: Solvents including dimethylsulfoxide (DMSO), ethylene glycol (EG), or glycerol (GLC) were trapped in bound complexes with APE1. The DMSO complex (PDB ID: 6MK3) was obtained by soaking preformed crystals in 5% DMSO overnight and then cryocooled in 100 mM

MES, pH 6.0, 200 mM NaCl, 22% PEG4000, 20-22% ethylene glycol, and 5% DMSO. The GLC complex (PDB ID: 6MKO) was obtained by soaking preformed crystals overnight in 1 mM macrocycle **20** and then cryocooling in the solvent above with 20% glycerol in place of ethylene glycol. All of the crystal cryocooled in ethylene glycol had multiple binding sites for this cryosolvent.

Other complexes: Two additional complexes were obtained from soaks. One including Tris and DMSO (PDB ID: 6MKM) was obtained from a soak that also included a reported arylstibonic acid inhibitor, compound 13755 from the NCI Diversity Set. In this case, the crystals were grown as described above and then soaked in 100 mM Tris pH 7.5, 200 mM NaCl, 1 mM 13755 (dissolved in DMSO resulting in a final concentration of 4% DMSO), and 20% PEG 3350. Crystals were cryocooled in 100 mM Tris-Cl, pH 7.5, 200 mM NaCl, 20% PEG 3350, 1 mM 13755, 4% DMSO, and 20% ethylene glycol. The second complex included Mg^{2+} and DMSO (PDB ID: 6MKK), obtained from a soak including 20 mM 4-hydroxymethyl phenyl acetic acid (Sigma Aldrich) along with 1 mM $MgCl_2$. Crystals were cryocooled in 100 mM MES, pH 6.0, 200 mM NaCl, 22% PEG4000, 20-22% ethylene glycol, 20 mM 4-(hydroxymethyl)-phenyl-acetic acid, and 4% DMSO. In each of these complexes, the inhibitor was not evident in the difference electron density map but DMSO was bound to the abasic sugar site with either Mg^{2+} or Tris in the metal binding site.

Data collection and processing: Data for all complexes except the GLC with C138A APE1 were collected at the GM/CA 23ID-D and SBC 19-BM beamlines at the Advanced Photon Source, Argonne National Laboratory and processed with HKL2000.[38] The GLC dataset was collected on our Bruker X8 Prospector (Bruker Corporation, Billerica, MA) with Cu Kα radiation (1.5418 Å) at 100 K by using an Oxford Cryosystem. Data were integrated using SAINT[39] and scaled with SADABS.[39] XPREP[39] was used to determine the space group and analyse the data. All of the crystals except the EG complex belong to $P2_12_12$ space group with cell dimensions as shown in Table 1. The EG complex crystal following the overnight soak belongs to space group $P2_1$. Apo, Mg^{2+} and Mn^{2+} bound structures have been previously reported.[28]

Structure Determination and Refinement. Phasing for the structures was obtained by molecular replacement (MOLREP) using the coordinates of C138A Δ40 hAPE1 as the search model. Several rounds of initial refinement were carried out using REFMAC5, accompanied by iterative model building using COOT. Following placement of well-ordered water molecules, excluding those in the repair active site of the enzyme, the bound solvent or metal was identified as a strong F_o-F_c difference peak. Final rounds of refinement for all of the structures were carried out by using PHENIX with isotropic temperature factor refinement. Statistics for refinements are compiled in Table 1.

Computational Methods. *Computational mapping and binding site identification.* Computational solvent mapping was performed using the FTMap algorithm through its online server (http://ftmap.bu.edu/) using magnesium bound (4QHE) and apo (4QHD) crystal structures of APE1, solved recently.[28] In brief, FTMAP simulates the interaction of the input protein structures with a library of 16 small organic probe molecules, with varying aromaticity, hydrophobicity and hydrogen bonding properties. For each probe in the library, the algorithm identifies 6 clusters, with lowest mean energy. Those clusters from different probes are further clustered into Consensus Sites (CS). Consensus sites are ranked by the number of its probe clusters. A detailed description of the method is provided in ([40]). It was observed experimentally that probes bind to the major binding sites of the protein. A detailed description of the method is provided in ([40, 41]). It was observed experimentally that probes bind to the major binding sites of the protein. We have also reported the FTSite approach, which uses FTMap results for binding site identification.[42] The method calculates percentage contact score for each consensus cluster. The method calculates the percentage contact score for each consensus cluster. The cluster having highest percentage contact score is considered core of the main site. The binding site is identified as all the consensus clusters within 12A from the core consensus site.

Docking and scoring of the compounds

Molecular docking of 105 macrocyclic compounds selected from the BU-CMD small molecule screening collection (http://cmd.bu.edu/) was performed on both the apo and Mg^{2+} bound structures using the Autodock program.[43] Initial conformations of macrocycles were generated with the Marvin program of

ChemAxon.[44] The Marvin Conformer plugin was used for generating 3D conformers of the macrocycles, and the Charge plugin was used for calculating partial charges prior to docking. The protein was held rigid during docking experiments. The docking box was selected to cover all mapping hot spots present in the site around largest consensus cluster. Initial conformations of macrocycles were generated with the Marvin program of ChemAxon. From the set of 100 conformations generated for each isomer, 10 lowest energy conformers were chosen. Preference was given to *trans* conformers of the peptide bond in the cycle. *Cis* conformers were only chosen if a set of 100 has less than 10 trans conformers. Conformer generation led to 1440 Autodock runs. Autodock was set to generate up to 10 clusters of docking poses. We chose the B site from two alternative positions of magnesium present in the 4QHE pdb structures. Ranking of the compounds was based on the average ensemble energy of the 50 lowest Autodock energy poses.

Apurinic/apyrimidinic endonuclease 1 assay. Macrocycles were tested for APE1 inhibition using a well characterized APE1 DNA repair activity assay performed in our laboratory and others.[45] The APE1 repair activity assay was performed in a 96-well plate assay using purified full-length APE1 enzyme and an AP site mimic consisting of two annealed oligonucleotides (5′-6-FAM-GCCCCC*GGGGACGTACGATATCCCGCTCC-3′ and 3′-Q-CGGGGGCCCCCTGCATGCTATAGGGCGAGG-5′) custom synthesized by Eurogentec Ltd. (Belgium). The oligonucleotides contained a quencher on one strand and a fluorescent 6-FAM label with an AP site mimic, tetrahydrofuran (*), on the complementary strand. The AP site mimic is a direct target of APE1's endonuclease function. Cleavage of the oligo at this site results in the release of the 6-FAM portion of the oligo from the complementary strand with the quencher. The amount of fluorescence due to this cleavage is directly proportional to APE1's endonuclease activity. Each macrocycle was tested in triplicate by a 1:2 serially diluted, 10-point dose scheme with 100 μM maximum concentrations in 200 μL final volume. A master mix was used providing a final amount of 50 nM annealed oligo, 50 mM Tris, 1 mM $MgCl_2$, and 50 mM NaCl, pH7.5. Due to the rapid enzymatic activity, 0.25-1.25 nM of full-length

APE1 was added to the wells at once and then immediately assayed. The fluorescence was read kinetically at five, one-minute intervals using a Bio-Tek Synergy H4® (Herman B Wells Center, Indiana University School of Medicine). The rate of the reaction was used to determine the change in APE1 repair activity as compared to the vehicle control (DMSO).

Cell cytotoxicity assays. Low passage patient-derived pancreatic cells (Pa02c)[46, 47] maintained in 10% FBS DMEM growth medium were plated at 2000 cells per well in poly-D-lysine treated 96-well clear bottom black plates and grown overnight in 5% CO_2 at 37 °C. Cells were then treated with 100 μL of macrocycle in doses made up in 5% FBS DMEM medium at 100 μM concentration and serially diluted 1:2 in a 5-point dose scheme. Wells dedicated to drug background and vehicle control (DMSO) were also included. Cells were grown for 48 hours in 5% CO_2 at 37 °C. Fresh 5% FBS DMEM medium was exchanged, and a fluorescent metabolic indicator, Alamar Blue® was added to each well at 10% final. After a 4 hour incubation in 5% CO_2 at 37 °C, plates were read on a Synergy H4™ (Bio-Tek). For each drug dose, background was subtracted and then further normalized to media alone. Data presented is percent normalized to media with mean standard error and includes vehicle (DMSO) response.

Alkaline comet assays. APE1 repair inhibitor candidates and APE1 repair inhibitor control, APE1 Repair Inhibitor III (ARiIII; Calbiochem), were tested in ST8814 at a single dose (100 μM or EC_{30}) and in combination with a single dose of MMS (1.0 mM) for a 1.0 hour treatment. Cells were seeded in 6-well tissue culture plates at 130,000 cells/well in DMEM + 10% FBS and grown overnight at 37 ºC, 5% CO_2. Media was exchanged with Opti-MEM™ (Gibco™) media containing Macrocycle alone or spiked with 1.0 mM MMS. Cells were then incubated for 1.0 hour at 37 ºC, 5% CO_2. Media was exchanged with PBS, and cells were treated with 0.25% Trypsin (HyClone™), collected, and washed with PBS. Cells were then counted by hemacytometer. DNA damage was evaluated by CometAssay® (Trevigen®) performed under alkaline conditions. Cells were resuspended in PBS at 1 x 10^5/mL, and then added to pre-melted and

cooled (37 °C) agarose at a 1:10 ratio. Cells were gently mixed, and then 50 µL of the agarose cell mix was transferred to pre-warmed comet slides (37 °C; CometSlide™). After solidifying at 4 °C, slides were placed in lysis solution for 60 minutes, and then placed in freshly prepared alkaline unwinding solution (NaOH; pH 13) for 20 minutes. Slides were then subjected to electrophoresis under alkaline conditions (NaOH; pH 13) at 1 Volt/cm (300 mA) for 30 minutes and then washed in H_2O, placed in 70% ethanol, and allowed to dry at 37 ºC for 30 minutes. Slides were stained with 100 µl of 1:10,000 diluted SYBR® Gold (Invitrogen™) in TE pH 7.5, and incubated for 30 minutes. Slides were then rinsed in H_2O briefly, and comets were captured by fluorescent microscope (Leica DMIL) and quantified by CometScore™ Pro (TriTec Corp®). DNA damage was measured by percent Tail DNA, and average values were obtained for 20 comet readings/macrocycle.

Chemistry.

General Methods: ^{1}H NMR spectra were recorded at 400 MHz or 500 MHz at ambient temperature with CD_3COCD_3 as the solvent unless otherwise stated. ^{13}C NMR spectra were recorded at 100 MHz or 125 MHz at ambient temperature with CD_3COCD_3 as the solvent unless otherwise stated. Chemical shifts are reported in parts per million. Data for ^{1}H NMR are reported as follows: chemical shift, multiplicity (app=apparent, br = broad, s = singlet, d =doublet, t = triplet, q = quartet, sxt = sextet, m = multiplet, ovrlp = overlap) coupling constants and integration. All ^{13}C NMR spectra were recorded with complete proton decoupling. High resolution mass spectra were obtained in the Boston University Chemical Instrumentation Center using a Waters Q-TOF mass spectrometer. Optical rotations were measured on all compounds for which sufficient material was available using a Rudolph Autopol II polarimeter. Analytical thin layer chromatography was performed using 0.25 mm silica gel 60-F plates. Flash chromatography was performed using 200-400 mesh silica gel (Sorbent Technologies, Inc.) or pre-pack column (SI-HC, puriFlash®) by Interchim puriFlash®450 or Yamazen Smart Flash EPCLC W-Prep2XY system. Isolated yields refer to chromatographically and spectroscopically pure compounds, unless otherwise stated. All reactions were carried out in oven-dried glassware under an argon atmosphere unless otherwise noted. Analytical LC-MS experiments were performed using a Waters Acquity UPLC (Ultra

Performance Liquid Chromatography) with a Binary solvent manager, SQ mass spectrometer, Waters 2996 PDA (Photo Diode Array) detector, and Evaporative Light Scattering Detector (ELSD). All microwave experiments were performed on a CEM Discover microwave reactor, using a sealed 10 or 35 mL vessel with temperatures monitored by an external sensor. All compounds tested in biological assays were determined to be >95% pure by UPLC-MS-ELSD analysis.

Tosyl-1*H*-pyrrole-2-carbaldehyde (3b): In a flame-dried, 250 mL round-bottomed flask equipped with an addition funnel under N_2, a suspension of sodium hydride (1.89 g, 47.33 mmol, 60% purity) was stirred in THF (24 mL). The reaction was cooled to 0 °C in an ice bath. A solution of 1H-pyrrole-2-carbaldehyde (3.00 g, 31.55 mmol) in THF (8 mL) was added steadily, dropwise, *via* addition funnel. An additional 4 mL THF was used to rinse the aldehyde solution vial and addition funnel. The ice bath was removed and the reaction was allowed to stir at room for 60 min. The tan suspension was then recooled to 0 °C, and a solution of 4-methylbenzenesulfonyl chloride (7.22 g, 37.86 mmol) in THF (12 mL) was added steadily, dropwise, *via* the addition funnel, which was then rinsed with an additional 12 mL THF. The resulting reddish-tan suspension was stirred at room temperature overnight. The reaction was quenched with water and poured into a separatory funnel containing ethyl acetate and water. The layers were separated and the organic layer was washed first with water, then brine. The organic layer was dried over Na_2SO_4, filtered and concentrated. The crude product was purified *via* silica plug, eluting with 15% ethyl acetate in hexanes (300 mL) and 30% ethyl acetate in hexanes (300 mL). The eluent was condensed and the resulting residue was recrystallized from ethyl acetate/hexanes to give off-white solid (3.69 g). ^{1}H NMR (400 MHz, $CDCl_3$) δ 9.97 (s, 1H), 7.80 (d, J = 8.2 Hz, 2H), 7.62 (dd, J = 2.9, 1.8 Hz, 1H), 7.32 (d, J = 8.2 Hz, 2H), 7.16-7.14 (m, 1H), 7.16 (dd, J = 3.5, 1.8 Hz, 1H), 6.40 (t, J = 3.2 Hz, 1H), 2.42 (s, 3H); ^{13}C NMR (101 MHz, $CDCl_3$) δ 145.9, 130.1,129.4, 127.4, 124.4, 112.4, 21.6; HRMS (ESI) m/z calcd. for $C_{12}H_{12}NO_3S$ $[M+H]^+$, 250.0538; found, 250.0537.

General procedure for the synthesis of enantioenriched Alloc-protected homoallylic amines 4: To a flame-dried, nitrogen-purged flask equipped with a stir bar was added allyl carbamate (1.0 equiv). Anhydrous dichloromethane was added, followed by the requisite aldehyde **14**-**18**. The reaction mixture was cooled to -78 °C and BF_3-diethyl etherate was slowly added via syringe. The reaction was stirred at -78 °C for 30 minutes. Crotylsilane **13** was added and the reaction vessel was transferred to a chiller set to -35 °C. The reaction was stirred at this temperature for 48-72 hours, tracking by TLC. Upon completion, the reaction mixture was carefully quenched with the addition of saturated aqueous sodium bicarbonate and extracted three times with dichloromethane. The combined organic fractions were washed with brine, dried over sodium sulfate, and condensed to give a crude product that was then purified by flash column chromatography.

Methyl (5*S*,6*R*,*E*)-6-(((allyloxy)carbonyl)amino)-5-methyl-6-phenylhex-3-enoate (4a). Obtained as a clear oil (90% yield, 10:1 dr) from aldehyde **3a** utilizing the general procedure. $[\alpha]^{25}_{D}$ +38 (*c* 0.39, $CHCl_3$); ^{1}H NMR (400 MHz, $CDCl_3$) δ = 7.24-7.16 (m, 2H), 7.16-7.10 (m, 3H), 5.81 (s, 2H), 5.46 (dt, *J* = 15.4, 6.6 Hz, 1H), 5.27 (dd, *J* = 15.4, 8.0 Hz, 1H), 5.19 (d, *J* = 16.8 Hz, 1H), 5.08 (d, *J* = 10.6 Hz, 1H), 4.58 (t, *J* = 7.4 Hz, 1H), 4.48 (dd, *J* = 13.3, 5.9 Hz, 1H), 4.41 (dd, *J* = 13.3, 4.3 Hz, 1H), 3.57 (s, 3H), 2.91 (d, *J* = 6.6 Hz, 2H), 2.56 (ddt, *J* = 8.0, 7.4, 7.0 Hz, 1H), 0.92 (d, *J* = 7.0 Hz, 3H); ^{13}C NMR (100MHz, $CDCl_3$) δ = 171.7, 155.2, 140.0, 135.2, 127.7, 126.9, 126.7, 123.0, 117.0, 65.0, 58.9, 51.4, 41.6, 37.3, 16.2; HRMS (m/z): $[M+Na]^+$ calcd. for $C_{18}H_{23}NO_4Na$, 340.1525; found, 340.1528.

Methyl (5*S*,6*R*,*E*)-6-(((allyloxy)carbonyl)amino)-5-methyl-6-(1-tosyl-1*H*-pyrrol-2-yl)hex-3-enoate (4b). Obtained as a clear oil (42% yield, >20:1 dr) from aldehyde **3b** utilizing the general procedure. $[\alpha]^{25}_{D}$ +41 (*c* 0.31, $CHCl_3$); ^{1}H NMR (400 MHz, $CDCl_3$) δ 7.74 (d, *J* = 7.6 Hz, 2H), 7.25 (d, *J* =7.6 Hz, 2H), 7.18 (br s, 1H), 6.17 (t, *J* = 2.7 Hz, 1H), 6.15-6.13 (m, 1H), 5.89 (ddd, *J* = 17.2, 11.0, 5.9, 5.5 Hz, 1H), 5.45 (dt, *J* = 15.6, 6.6 Hz, 1H), 5.37 (dd, *J* = 15.6, 6.6 Hz, 1H), 5.26 (d, *J* = 17.2 Hz, 1H), 5.22-5.10 (m, 3H), 4.51 (dd, *J* = 13.5, 5.5 Hz, 1H), 4.46 (dd, *J* = 13.5, 5.9 Hz, 1H), 3.65 (s, 3H), 2.94 (d, *J* = 6.6 Hz, 2H), 2.80 (sxt,

J = 6.5 Hz, 1H), 2.37 (s, 3H), 0.95 (d, J = 6.6 Hz, 3H); ^{13}C NMR (100 MHz, $CDCl_3$) δ 171.8, 154.9, 144.5, 135.8, 135.3, 134.5, 132.4, 132.2, 129.5, 126.5, 123.0, 122.5, 117.2, 113.6, 111.5, 76.4, 65.2, 51.9, 51.4, 40.8, 37.5, 21.2, 14.8. HRMS (m/z): $[M+Na]^+$ calcd. for $C_{23}H_{28}N_2O_6SNa$, 483.1566; found, 483.1579.

Methyl (5*S*,6*R*,*E*)-6-((*S*)-2-((*tert*-butoxycarbonyl)amino)-3-(1*H*-Indol-3-yl)propanamido)-5-methyl-6-phenylhex-3-enoate (7a): In a 50 mL round-bottomed flask under N_2 was stirred **4a** (394.00 mg, 1.24 mmol, 1.0 equiv) in CH_2Cl_2 (4.5 mL) and methanol (1.5 mL). Dimethylbarbituric acid (242 mg, 1.55 mmol, 1.25 equiv) was then added, followed by Tetrakis(triphenylphosphine)palladium(0) (85.97 mg, 74.40 μmol, 6 mol%). The reaction was stirred at room temperature for four hours, forming a dark orange-reddish solution. MP-TsOH (65) resin (Biotage, Inc.) was added (1.6 g; 4.96 mmol; 4 equiv; loading: 3.11 mmol/g) in one portion. The reaction was diluted with CH_2Cl_2 (3 mL) to allow for better mixing of resin. The resulting suspension was stirred at room temperature for two hours. The resin was then filtered off and rinsed with CH_2Cl_2 (5 x 10 mL). The resin was then transferred to a round-bottomed flask and suspended in CH_2Cl_2 (20 mL). To the suspension was added Et_3N (5.5 mL). The mixture was stirred at room temperature for 30 min. The resin was then filtered off and rinsed with CH_2Cl_2 (4 x 5 mL), retaining the mother liquor. The resin was re-treated with 20 mL CH_2Cl_2 and 5 mL Et_3N for 20 minutes and filtered again, rinsing with 3 x 5 mL CH_2Cl_2. The combined mother liquors from both treatments were concentrated to afford the deprotected amine **5a** that was carried forward to the next step without further purification.

Compound **5a** and Boc-L-tryptophan (434.60 mg, 1.43 mmol, 1.5 equiv) were combined in CH_2Cl_2 (6 mL). HATU (542.97 mg, 1.43 mmol, 1.5 equiv) was then added, followed by Hunig's base (384.49 mg, 2.97 mmol, 2.4 equiv). The reaction was stirred at room temperature for 3.5 hours. The solvent was removed in vacuo, and the crude residue was purified by flash chromatography (SiO_2, gradient elution 35-45% ethyl acetate in hexanes) to give product **7a** (451 mg; 72.9% yield over two steps). $[\alpha]^{25}_D$ +29 (*c*

0.20, $CHCl_3$); ^1H NMR (400 MHz, acetone-d_6) δ 10.05 (br s, 1H), 7.61 (d, *J* = 7.8 Hz, 1H), 7.35 (br d, *J* = 7.8 Hz, 2H), 7.27-7.20 (m, 4H), 7.19-7.14 (m, 1H), 7.13-7.04 (m, 2H), 6.99 (br t, *J* = 7.2 Hz, 1H), 5.98 (br d, *J* = 7.0 Hz, 1H), 5.24 (br d, *J* = 2.3 Hz, 2H), 4.82 (br t, *J* = 7.6 Hz, 1H), 4.50-4.37 (m, *J* = 14.3, 7.0 Hz, 1H), 3.56 (s, 3H), 3.21 (dd, *J* = 14.3, 6.6 Hz, 1H), 3.09 (dd, *J* = 14.3, 7.0 Hz, 1H), 2.86 (br s, 2H), 2.47-2.35 (m, *J* = 6.6 Hz, 1H), 1.33 (br s, 9H), 0.82 (br d, *J* = 6.6 Hz, 3H); ^{13}C NMR (101 MHz, acetone-d_6) δ 206.4, 172.4, 171.8, 156.3, 141.8, 137.6, 136.4, 128.8, 128.6, 128.4, 127.6, 124.4, 124.2, 122.1, 119.5, 119.5, 112.2, 112.2, 111.5, 79.4, 58.0, 56.4, 51.9, 42.4, 38.0, 29.0, 28.6, 16.7; HRMS (ESI) m/z calcd. for $C_{30}H_{37}N_3O_5Na$ $[M+Na]^+$, 542.2631; found, 542.2630.

Methyl (5*S*,6*R*,*E*)-6-((*S*)-2-((*tert*-butoxycarbonyl)amino)-3-(1*H*-indol-3-yl)propanamido)-5-methyl-6-(1-tosyl-1*H*-pyrrol-2-yl)hex-3-enoate (7b): In a 100 mL round-bottomed flask under N_2, **4b** (1.10 g, 2.39 mmol, 1.0 equiv) was dissolved in in CH_2Cl_2 (9 mL) and methanol (4 mL). Dimethyl barbituric acid (447.53 mg, 2.87 mmol, 1.2 equiv) was then added, followed by tetrakis(triphenylphosphine) palladium(0) (165.60 mg, 143.31 μmol, 6 mol%). The reaction was stirred at room temperature for four hours. The dark orange reaction was then diluted with CH_2Cl_2 (5 mL), and MP-TsOH (65) resin (Biotage, Inc.) (3.1 g; 9.56 mmol; 4 equiv ; loading: 3.11 mmol/g) was added. The reaction was stirred at room temperature for two hours. The resin was filtered off and rinsed with CH_2Cl_2 (4 x 5 mL), 10% MeOH/CH_2Cl_2 (2 x 20 mL), CH_2Cl_2 (2 x 5 mL).

The resin was then then returned to the round-bottom flask and dissolved in CH_2Cl_2 (20 mL). Et_3N (5 mL) was added, and the suspension was stirred at room temperature for 1.25 hrs. The resin was filtered off and rinsed with CH_2Cl_2 (4 x 10 mL), retaining the mother liquor. The resin was then re-treated with CH_2Cl_2 (20 mL) and Et_3N (5 mL) for 45 minutes. The resin was again filtered off, rinsing with CH_2Cl_2 (3 x 5 mL). The combined mother liquors from both treatments were concentrated to afford the deprotected amine **5b**, which was carried forward to the next step without further purification.

In a 100 mL round bottomed flask, amine **5b** was stirred with Boc-L-tryptophan (836.33 mg, 2.75 mmol, 1.15 equiv) in CH_2Cl_2 (11 mL). HATU (957.80 mg, 2.52 mmol, 1.05 equiv) was then added,

followed by Hunig's base (739.9 mg, 5.73 mmol, 999.86 µL, 2.4 equiv). The reaction was stirred at room temperature overnight. The reaction was then diluted with CH_2Cl_2 and washed with water. The organic layer was dried over Na_2SO_4, filtered and concentrated. The crude residue was purified by flash chromatography (SiO_2; gradient elution 38-48% ethyl acetate in hexanes.) to give product **7b** (1.09 g, 71.8% yield over two steps). $[\alpha]^{25}_D$ +34 (*c* 0.22, $CHCl_3$); ^{1}H NMR (400 MHz, acetone-d_6) δ 10.07 (br s, 1H), 7.95 (br d, *J* = 8.2 Hz, 2H), 7.62 (d, *J* = 7.8 Hz, 1H), 7.38 (br d, *J* = 8.2 Hz, 3H), 7.29 (br d, *J* = 9.0 Hz, 1H), 7.15 (br d, *J* = 1.6 Hz, 2H), 7.09 (t, *J* = 7.4 Hz, 1H), 7.00 (t, *J* = 7.4 Hz, 1H), 6.26-6.15 (m, 2H), 5.99 (br d, *J* = 7.2 Hz, 1H), 5.86-5.76 (m, 1H), 5.50-5.26 (m, 2H), 4.49-4.38 (m, 1H), 3.60 (s, 3H), 3.25 (dd, *J* = 14.5, 6.3 Hz, 1H), 3.08 (br dd, *J* = 14.3, 7.2 Hz, 1H), 2.93 (br s, 2H), 2.63 (br d, *J* = 5.5 Hz, 1H), 2.39 (s, 3H), 1.35 (br s, 9H), 0.87 (br d, *J* = 6.6 Hz, 3H); ^{13}C NMR (101 MHz, $CDCl_3$) δ 170.8, 145.2, 136.5, 136.0, 130.1, 127.3, 123.4, 122.5, 119.9, 119.2, 114.2, 112.2, 111.5, 52.2, 37.9, 28.6, 21.9; HRMS (ESI) m/z calcd. for $C_{35}H_{42}N_4O_7SNa$ $[M+Na]^+$, 685.2672; found, 685.2673.

Macrocyclic library synthesis. Macrocycles employed in the primary screen were synthesized according to the general procedure for macrolactone synthesis outlined below. Crude reaction mixtures were directly purified using mass-guided, preparative HPLC on a Waters FractionLynx system. Purified compounds meeting a >90% purity threshold (as determined by UPLC-MS-ELSD) were stored as 20 mM DMSO stocks at -30 °C prior to aliquotting for screening.

General procedure for macrolactone library synthesis (MC001-MC105): In a 25 mL round-bottomed flask was stirred Boc-protected amine **7** (0.57 mmol) in CH_2Cl_2 (6 mL). A solution of 4.0 M HCl in dioxane (0.86 mL, 6.0 equiv) was added. The reaction was stirred at room temperature for 3.25 hours. The solvent was evaporated, and the residue was azeotroped four times with CH_2Cl_2 (4 mL portions). The resultant gum was then taken up in CH_2Cl_2 (5 mL). MP-Carbonate resin (Biotage, Inc.) was added (0.31 g; 0.89 mmol; 3.6 equiv; 2.9mmol/g loading). The suspension was stirred at room temperature for 1.5 hours. The resin was filtered off and rinsed with CH_2Cl_2 (3 x 4 mL). The mother liquor was evaporated,

and the residue was transferred to a 10 mL microwave vessel using trifluorotoluene (1.2 mL). Lactone **9** (6.0 equiv) was added, followed by Otera's catalyst (15 mol%). The vessel was capped and heated in the microwave at 175 °C for 45 min. For the original macrocycle library, the solvent was removed using centrifugal evaporation and the resultant residues were dissolved in DMSO and purified *via* mass-guided preparative HPLC. For follow-on syntheses and characterizations, the reaction suspension was directly loaded onto a silica/celite column (pre-wet with 20% acetone/H) using CH_2Cl_2. Elution with a gradient of 20% acetone/hexanes, (40 mL), 30% acetone/hexanes (20 mL), 40% acetone/hexanes (20 mL), 50% acetone/hexanes (20 mL), 60% acetone/hexanes (20 mL) afforded the analytically pure macrolactone.

Synthetic yields and full characterization data for macrolactones 10-13:

(7*S*,10*R*,11*S*,*E*)-7-((1*H*-indol-3-yl)methyl)-11-methyl-10-phenyl-1-oxa-6,9-diazacyclopentadec-12-ene-5,8,15-trione (10): Macrolactone **10** was obtained from Boc-amine **7a** and lactone **9a** according to the general procedure (29.8% yield over two steps). $[\alpha]^{25}_D$ +7 (*c* 0.13, $CHCl_3$); ^{1}H NMR (400 MHz, acetone-d_6) δ 10.01 (br s, 1H), 7.56 (d, J = 7.8 Hz, 1H), 7.37-7.20 (m, 8H), 7.17-7.02 (m, 2H), 6.98 (t, *J* = 7.8 Hz, 1H), 5.60 (ddd, *J* = 15.2, 8.6, 5.9 Hz, 1H), 5.14 (dd, *J* = 15.2, 9.2 Hz, 1H), 4.94 (dd, *J* = 7.8, 3.1 Hz, 1H), 4.82-4.72 (m, 1H), 4.33-4.24 (m, 1H), 3.36 (d, *J* = 15.0, 3.1 Hz, 1H), 3.10 (d, *J* = 15.0, 8.5 Hz, 1H), 3.03 (dd, *J* = 16.0, 5.9 Hz, 1H), 2.96 (dd, *J* = 16.0, 8.6 Hz, 1H), 2.69-2.59 (m, 1H), 2.42-2.32 (m, 1H), 2.31-2.20 (m, 2H), 1.76-1.65 (m, 1H), 0.87 (d, *J* = 6.3 Hz, 3H); ^{13}C NMR (101 MHz, acetone-d_6) δ 173.9, 172.5, 171.8, 140.2, 138.2, 136.4, 129.3, 129.3, 129.6, 129.1, 128.5, 128.3, 126.2, 125.2, 124.7, 124.5, 122.7, 120.2, 120.1, 119.8, 112.7, 112.5, 67.0, 58.7, 56.0, 42.1, 40.0, 35.0, 28.3, 24.2, 18.2; HRMS (ESI) m/z calcd. for $C_{28}H_{31}N_3O_4Na$ $[M+Na]^+$, 496.2212; found, 496.2223

(8*S*,11*R*,12*S*,*E*)-8-((1*H*-indol-3-yl)methyl)-12-methyl-11-phenyl-1-oxa-7,10-diazacyclohexadec-13-ene-6,9,16-trione (11): Macrolactone **11** was obtained from Boc-amine **7a** and lactone **9i** according to the general procedure (32% yield over two steps). $[\alpha]^{25}_D$ -24 (*c* 0.17, $CHCl_3$); ^{1}H NMR (400 MHz, acetone-d_6) δ 9.99 (br s, 1H), 7.49 (d, *J* = 8.2 Hz, 1H), 7.45 (d, *J* = 8.2 Hz, 1H), 7.37-7.22 (m, 7H), 7.07 (t, *J* = 7.6

Hz, 1H), 6.96 (t, *J* = 7.0 Hz, 1H), 6.87 (br s, 1h), 5.71 (ddd, *J* = 15.5, 10.0, 4.3, 1H), 5.26 (dd, *J* = 15.5, 9.0 Hz, 1H), 4.93 (dd, *J* = 8.2, 3.5 Hz, 1H), 4.78 (td, *J* = 8.0, 4.5 Hz, 1H), 4.24 (td, *J* = 10.5, 3.3 Hz, 1H), 4.01 (dt, *J* = 10.5, 4.7 Hz, 1H), 3.19 (dd, *J* = 15.0, 4.5 Hz, 1H), 3.11 (dd, *J* = 15.0, 8.0 Hz, 1H), 3.09 (dd, *J* = 15.0, 6.6 Hz), 2.9-2.7 (m, 2H, obsc.), 2.65-2.56 (m, 1H), 2.23 (td, *J* = 9.4, 4.7 Hz, 1H), 1.95-1.85 (m, 1H), 1.80-1.65 (m, 2H), 1.65-1.57 (m, 1H), 0.92 (t, *J* = 7.0 Hz, 3H); ^{13}C NMR (101 MHz, acetone-d_6) δ 173.0, 170.8, 170.7, 139.8, 136.8, 134.2, 128.6, 128.4, 127.8, 127.2, 124.9, 123.8, 121.5, 119.0, 118.6, 111.5, 62.4, 57.5, 54.4, 41.9, 40.8, 39.2, 34.1, 27.4, 27.2, 21.8, 18.1; HRMS (ESI) m/z calcd. for $C_{29}H_{33}N_3O_4Na$ $[M+Na]^+$, 510.2369; found, 510.2354.

(7*S*,10*R*,11*S*,*E*)-7-((1*H*-indol-3-yl)methyl)-11-methyl-10-(1-tosyl-1*H*-pyrrol-2-yl)-1-oxa-6,9-diazacyclopentadec-12-ene-5,8,15-trione (12): Macrolactone **12** was obtained from Boc-amine **7b** and lactone **9a** according to the general procedure (36.9% yield over two steps). $[\alpha]^{25}_D$ +5 (*c* 0.526, $CHCl_3$); ^{1}H NMR (500 MHz, acetone-d_6) δ 10.02 (br s, 1H), 7.94 (d, *J* = 8.2 Hz, 2H), 7.60 (d, *J* = 7.8 Hz, 1H), 7.42 (d, *J* = 8.2 Hz, 2H), 7.36 (d, *J* = 8.2 Hz, 1H), 7.30 (br s, 1H), 7.13-7.04 (m, 3H), 7.00 (t, *J* = 7.8 Hz, 1H), 6.32 (br s, 1H), 6.28 (t, *J* = 3.1 Hz, 1H), 5.94 (dd, *J* = 8.8, 4.1 Hz, 1H), 5.52 (dt, *J* = 15.2, 7.4, 7.4 Hz, 1H), 5.38 (dd, *J* = 15.2, 7.8 Hz, 1H), 4.68 (ddd, *J* = 10.6, 7.8, 3.5 Hz, 1H), 4.23-4.15 (m, 1H), 4.06 (t, *J* = 9.4 Hz, 1H), 3.44 (dd, *J* = 15.0, 3.5 Hz, 1H), 3.03-2.95 (m, 2H), 2.89 (dd, J = 15.0, 10.6 Hz, 1H), 2.74-2.63 (m, 1H), 2.39 (s, 3H), 2.34-2.20 (m, 1H), 2.20-2.07 (m, 2H), 1.66-1.53 (m, 1H), 0.90 (d, *J* = 7.0 Hz, 3H); ^{13}C NMR (101 MHz, acetone-d_6) δ 173.9, 173.0, 171.8, 146.8, 138.2, 137.8, 136.7, 134.9, 131.6, 128.8, 126.3, 124.6, 124.1, 122.8, 120.2, 119.8, 116.0, 113.5, 112.8, 112.7, 66.9, 56.4, 50.1, 41.6, 39.9, 35.1, 29.0, 24.3, 22.1, 17.1; HRMS (ESI) m/z calcd. for $C_{33}H_{36}N_4O_6SNa$ $[M+Na]^+$, 639.2253; found, 639.2248.

(8*S*,11*R*,12*S*,*E*)-8-((1*H*-indol-3-yl)methyl)-12-methyl-11-(1-tosyl-1*H*-pyrrol-2-yl)-1-oxa-7,10-diazacyclohexadec-13-ene-6,9,16-trione (13): Macrolactone **13** was obtained from Boc-amine **7b** and

lactone **9i** according to the general procedure (30.5% yield over two steps). $[\alpha]^{25}_{D}$ -29 (*c* 0.32, $CHCl_3$); ^{1}H NMR (400 MHz, acetone-d_6) δ 9.99 (br s, 1H), 8.06 (d, *J* = 8.0 Hz, 2H), 7.50 (d, *J* = 7.8 Hz, 1H), 7.82 (d, *J* = 8.0 Hz, 2H), 7.42-7.37 (m, 1H), 7.35 (d, *J* = 8.2 Hz, 1H), 7.23 (dd, *J* = 3.1, 2.0 Hz, 1H), 7.17 (br d, *J* = 8.2 Hz, 1H), 7.06 (t, *J* = 7.6 Hz, 1H), 6.95 (br s, 1H), 6.93 (t, *J* = 7.0 Hz, 1H), 6.25-6.20 (m, 2H), 5.94 (dd, *J* = 8.2, 3.5 Hz, 1H), 5.63 (ddd, *J* = 16.0, 6.0, 5.0 Hz, 1H), 5.54 (dd, *J* = 16.0, 6.3 Hz, 1H), 4.70 (td, *J* = 9.0, 4.0 Hz, 1H), 4.18 (ddd, *J* = 10.9, 9.0, 4.3 Hz, 1H), 4.12 (dd, *J* = 10.9, 5.1 Hz, 1H), 3.20 (dd, *J* = 15.4, 4.0 Hz, 1H), 3.09 (dd, *J* = 15.4, 9.0 Hz, 1H), 3.02 (d, *J* = 5.9 Hz, 1H), 3.00 (d, *J* = 6.3 Hz, 1H), 2.77-2.70 (m, 1H), 2.37 (s, 3H), 2.21 (dt, *J* = 14.3, 7.4 Hz, 1H), 1.98 (dt, *J* = 14.3, 7.8 Hz, 1H), 1.90-1.80 (m, 1H), 1.70-1.60 (m, 2H), 1.60-1.50 (m, 1H), 0.93 (d, *J* = 7.0 Hz, 3H); ^{13}C NMR (101 MHz, acetone-d_6) δ 173.1, 171.4, 171.2, 145.5, 137.0, 136.8, 134.9, 130.3, 128.2, 127.8, 124.2, 123.7, 123.3, 121.6, 119.1, 118.7, 114.9, 112.6, 111.6, 110.9, 62.7, 55.4, 49.7, 41.0, 38.7, 34.4, 27.9, 27.7, 21.9, 21.0, 15.3; HRMS (ESI) m/z calcd. for $C_{34}H_{39}N_4O_6S$ $[M+H]^+$, 631.2590; found, 631.2586.

Synthetic procedures and full characterization data for macrolactams 17-32.

Part A: General procedure for amino acid coupling: In a 25 mL round-bottomed flask, compound **7a**/**7b** (0.576 mmol, 1.0 equiv) was dissolved in CH_2Cl_2 (6 mL). A solution of 4.0 M HCl in dioxane (0.86 mL, 6.0 equiv) was then added. The reaction was stirred at room temperature for 3.25 hours, at which time the solvent was removed *in vacuo*. The resultant residue was azeotroped four times with 4 mL portions of CH_2Cl_2 to afford **8a**/**8b** as a foamy gum. This crude gum was then dissolved in CH_2Cl_2 (1 mL) in a 25 mL round-bottomed flask. The appropriate Boc-amino acid **14a-k** (1.1 equiv) was added, followed by HATU (1.1 equiv) and Hunig's base (2.0 equiv). After stirring at room temperature for four hours, the reaction mixture was concentrated *in vacuo* and the crude residue was directly purified by flash column chromatography using a gradient elution of 25-45% acetone in hexanes to afford the Boc-protected intermediate **15/16**.

Several of the Boc-protected intermediates exhibited significant peak splitting, possibly due to the presence of Boc rotamers. In addition, several Boc intermediates were not sufficiently pure for characterization, and were carried on to the next step (Part B) without further attempts to purify. Only the Boc-intermediates of sufficient purity for characterization are described below.

Part B: General procedure for three-step deprotection/cyclization sequence: Intermediate **15/16** (0.105 mmol) was dissolved in methanol (1 mL). A solution of 2.5M aqueous NaOH (1.5 equiv) was then added, and the reaction was stirred at room temperature overnight. The solvent was removed *in vacuo* and the residue was dissolved in THF (1 mL). The solution was acidified *via* addition of 1N HCl (0.13 mL). The mixture was stirred for two minutes and the solvent was removed *in vacuo*. The residue was then dissolved in CH_2Cl_2 and the solution was passed through an Isolute HM-N cartridge, eluting with additional CH_2Cl_2. The solution was concentrated in a 25 mL round-bottom flask and 1 mL CH_2Cl_2 was added, followed by a solution of 4.0N HCl in dioxane (5.0 equiv). The reaction was stirred at room temperature for three hours and then concentrated *in vacuo*. The resulting residue was azeotroped four times with CH_2Cl_2, and transferred to a two dram vial in DMF (1.2 mL). To this solution was added HATU (1.75 equiv), followed by Hunig's base (4.0 equiv). The reaction was stirred at room temperature overnight. The solvent was removed *in vacuo* and the crude residue was purified by flash column chromatography (SiO2; gradient elution 20-60% acetone in hexanes) to afford the macrolactam product.

Methyl (6S,10S,13R,14S,E)-10-((1H-indol-3-yl)methyl)-6-(4-fluorophenyl)-2,2,14-trimethyl-4,8,11-trioxo-13-phenyl-3-oxa-5,9,12-triazaoctadec-15-en-18-oate (15i): 77% yield from **7a,** after deprotection and coupling to **14i**, according to the general procedure, part A. $[\alpha]^{25}_{D}$ +16 (*c* 0.146, $CHCl_3$); ^{1}H NMR (400 MHz, acetone-d_6) δ 10.11 (br s, 1H), 7.66 (br d, *J* = 7.8 Hz, 1H), 7.47 (br d, *J* = 7.4 Hz, 1H), 7.39 (br d, *J* = 7.8 Hz, 3H), 7.34-7.08 (m, 9H), 7.04 (br t, *J* = 7.4 Hz, 1H), 6.95 (br t, *J* = 8.6 Hz,1H), 6.83 (br d, *J* = 6.3 Hz, 1H), 5.18-4.97 (m, 3H), 4.83-4.69 (m, 2H), 3.59 (s, 3H), 3.17-3.03 (m, 2H), 2.81 (br d, *J* = 6.3 Hz, 2H), 2.62-2.49 (m, 2H), 2.28-2.16 (m, 1H), 1.36 (br s, 9H), 0.73 (br d, *J* = 6.3 Hz, 3H); ^{13}C NMR (101 MHz, acetone-d_6) δ 172.5, 171.1, 170.7, 162.6 (d, $J_{C\text{-}F}$=242.8 Hz, 1 C), 155.8,

141.8, 137.7, 136.2, 129.1, 129.0, 128.8, 128.7 (2 C), 128.5 (2 C), 127.7, 124.5 (2 C), 124.4 (2 C), 122.3, 119.7, 119.7, 115.7 (d, J_{C-F}=21.4 Hz, 2 C), 112.3, 111.6, 79.1, 58.2, 55.3, 52.4, 52.0, 43.1, 42.4, 38.0, 28.7, 17.0; HRMS (ESI) m/z calcd. for $C_{39}H_{46}FN_4O_6$ $[M+H]^+$, 685.3401; found, 685.3389.

Methyl (6S,10S,13R,14S,E)-10-((1H-indol-3-yl)methyl)-6-(4-chlorophenyl)-2,2,14-trimethyl-4,8,11-trioxo-13-phenyl-3-oxa-5,9,12-triazaoctadec-15-en-18-oate (15j): 78% yield from **7a,** after deprotection and coupling to **14j**, according to the general procedure, part A. $[\alpha]^{25}_D$ +13 (*c* 0.173, $CHCl_3$); ^{1}H NMR (400 MHz, acetone-d_6) δ 10.06 (br s, 1H), 7.64 (d, *J* = 7.8 Hz, 1H), 7.39 (br d, *J* = 7.8 Hz, 1H), 7.32-7.14 (m, 11H), 7.14-7.08 (m, 2H), 7.04 (t, *J* = 7.1 Hz, 1H), 6.82 (br s, 1H), 5.21-4.94 (m, 3H), 4.79-4.63 (m, 2H), 3.60 (s, 3H), 3.06 (br d, *J* = 7.0 Hz, 2H), 2.73 (s, 3H), 2.62 (br d, *J* = 9.8 Hz, 1H), 2.30-2.13 (m, 1H), 1.36 (br s, 9H), 0.74 (br d, *J* = 7.0 Hz, 3H); ^{13}C NMR (101 MHz, $CDCl_3$) δ 172.2, 169.8, 169.7, 154.9, 138.6, 135.9, 134.6, 132.5, 128.2, 127.6, 127.1, 127.0, 126.8, 123.4, 122.8, 121.9, 119.3, 118.4, 111.1, 110.3, 79.3, 56.8, 54.0, 51.6, 41.6, 41.0, 38.3, 36.9, 29.3, 28.5, 28.0, 16.3; HRMS (ESI) m/z calcd. for $C_{39}H_{45}ClN_4O_6Na$ $[M+Na]^+$, 723.2925; found, 723.2924.

Methyl (11S,14R,15S,E)-11-((1H-indol-3-yl)methyl)-2,2,15-trimethyl-4,9,12-trioxo-14-(1-tosyl-1H-pyrrol-2-yl)-3-oxa-5,10,13-triazanonadec-16-en-19-oate (16a): 81% yield from **7b,** after deprotection and coupling to **14a**, according to the general procedure, part A. $[\alpha]^{25}_D$ +17 (*c* 0.14, $CHCl_3$); ^{1}H NMR (400 MHz, acetone-d_6) δ 10.04 (br s, 1H), 7.91 (br d, *J* = 8.2 Hz, 2H), 7.60 (d, *J* = 7.8 Hz, 1H), 7.38 (br d, *J* = 9.0 Hz, 1H), 7.36-7.29 (m, 4H), 7.14 (br s, 2H), 7.09-7.02 (m, 1H), 7.01-6.92 (m, 1H), 6.16 (br s, 1H), 6.13 (t, *J* = 3.3 Hz, 1H), 5.94 (br s, 1H), 5.77 (dd, *J* = 8.8, 5.7 Hz, 1H), 5.41-5.22 (m, 2H), 4.73 (q, *J* = 7.4 Hz, 1H), 3.56 (s, 3H), 3.24 (dd, *J* = 14.9, 6.3 6Hz, 1H), 3.05 (dd, *J* = 14.5, 7.4 Hz, 1H), 2.97-2.83 (m, 4H), 2.63-2.52 (m, 1H), 2.33 (s, 3H), 2.15-2.08 (m, 2H), 1.71-1.56 (m, 1H), 1.70-1.55 (m, 1H), 1.72-1.55 (m, 2H), 1.35 (s, 9H), 0.83 (d, *J* = 6.6 Hz, 3H); ^{13}C NMR (101 MHz, acetone-d_6) δ 173.5, 172.9, 172.3, 146.5, 138.0, 137.7, 136.9, 136.7, 131.3, 129.2, 128.5, 124.8, 124.4, 124.1, 122.6, 120.0, 119.9, 115.3, 113.5, 112.6, 112.0, 79.0, 55.2, 52.3, 51.2, 43.1, 41.0, 38.6, 34.3, 31.1, 30.9, 30.7, 30.5, 30.1, 30.0, 29.8,

30.3, 29.2, 27.4, 22.0, 15.8; HRMS (ESI) m/z calcd. for $C_{39}H_{49}N_5O_8SNa$ $[M+Na]^+$, 770.3200; found, 770.3185.

Methyl (12S,15R,16S,E)-12-((1H-indol-3-yl)methyl)-2,2,16-trimethyl-4,10,13-trioxo-15-(1-tosyl-1H-pyrrol-2-yl)-3-oxa-5,11,14-triazaicos-17-en-20-oate (16b): 74% yield from **7b,** after deprotection and coupling to **14b**, according to the general procedure, part A. $[\alpha]^{25}_D$ +19 (*c* 0.14, $CHCl_3$); ^{1}H NMR (400 MHz, acetone-d_6) δ 10.05 (br s, 1H), 7.90 (d, *J* = 8.2 Hz, 2H), 7.61 (d, *J* = 7.8 Hz, 1H), 7.40-7.29 (m, 4H), 7.23 (br d, *J* = 7.8 Hz, 1H), 7.15 (d, *J* = 1.6 Hz, 2H), 7.06 (t, *J* = 1.0 Hz, 1H), 6.98 (t, *J* = 1.0 Hz, 1H), 6.19-6.10 (m, 2H), 5.82 (br s, 1H), 5.76 (dd, *J* = 9.0, 5.5 Hz, 1H), 5.36-5.30 (m, 2H), 4.73 (q, *J* = 7.6 Hz, 1H), 3.56 (s, 3H), 3.24 (dd, *J* = 14.5, 6.6 Hz, 1H), 3.04 (dd, *J* = 14.5, 7.8 Hz, 1H), 2.97-2.84 (m, 4H), 2.64-2.50 (m, 1H), 2.33 (s, 3H), 2.13-2.07 (m, 2H), 1.55-1.41 (m, 2H), 1.36 (s, 9H), 1.33-1.22 (m, 2H), 0.82 (d, *J* = 7.0 Hz, 3H); ^{13}C NMR (101 MHz, acetone-d_6) δ 173.3, 172.5, 171.9, 156.7, 146.1, 137.6, 137.2, 136.4, 136.3, 130.9, 128.8, 128.1, 124.4, 124.0, 123.7, 122.2, 119.6, 119.5, 114.9, 113.1, 112.2, 112.2, 111.6, 78.4, 54.7, 51.9, 50.7, 42.5, 40.7, 38.2, 36.2, 30.7, 28.8, 23.5, 21.6, 15.3; HRMS (ESI) m/z calcd. for $C_{40}H_{51}N_5O_8SNa$ $[M+Na]^+$, 784.3356; found, 784.3343.

Methyl (10S,13R,14S,E)-10-((1H-indol-3-yl)methyl)-2,2,14-trimethyl-4,8,11-trioxo-13-(1-tosyl-1H-pyrrol-2-yl)-3-oxa-5,9,12-triazaoctadec-15-en-18-oate (16c): 93% yield from **7b,** after deprotection and coupling to **14c**, according to the general procedure, part A. $[\alpha]^{25}_D$ +19 (*c* 0.27, $CHCl_3$); ^{1}H NMR (400 MHz, acetone-d_6) δ 10.06 (br s, 1H), 7.90 (d, *J* = 8.2 Hz, 2H), 7.61 (d, *J* = 7.8 Hz, 1H), 7.42-7.29 (m, 5H), 7.15 (br s, 2H), 7.10-7.02 (m, 1H), 6.92-7.02 (m, 1H), 6.19-6.12 (m, 2H), 5.85 (br s, 1HN), 5.76 (br dd, *J* = 9.0, 5.5 Hz, 1H), 5.35-5.28 (m, 2H), 4.72 (q, *J* = 7.2 Hz, 1H), 3.56 (s, 3H), 3.30-3.15 (m, 3H), 3.13-3.00 (m, 1H), 2.88 (br d, *J* = 5.5 Hz, 2H), 2.64-2.50 (m, 1H), 2.33 (s, 3H), 2.36-2.23 (m, 2H), 1.34 (s, 9H), 0.82 (d, *J* = 6.6 Hz, 3H); ^{13}C NMR (101 MHz, acetone-d_6) δ 172.9, 172.4, 172.1, 172.1, 157.0, 146.5, 138.0, 137.7, 136.7, 131.3, 129.2, 128.6, 124.9, 124.8, 124.4, 124.1, 124.1, 122.7, 120.0, 120.0,

115.3, 113.6, 112.7, 112.6, 112.0, 79.2, 55.2, 52.3, 51.2, 43.0, 39.2, 38.6, 38.2, 37.1, 29.3, 29.1, 22.0, 15.8; HRMS (ESI) m/z calcd. for $C_{38}H_{47}N_5O_8SNa$ $[M+Na]^+$, 756.3043; found, 756.3033.

Methyl (6S,10S,13R,14S,E)-10-((1H-Indol-3-yl)methyl)-2,2,14-trimethyl-4,8,11-trioxo-13-(1-tosyl-1H-pyrrol-2-yl)-6-(4-(trifluoromethyl)phenyl)-3-oxa-5,9,12-triazaoctadec-15-en-18-oate (16g): 70% yield from **7b,** after deprotection and coupling to **14g**, according to the general procedure, part A. $[\alpha]^{25}_D$ +3 (*c* 0.36, $CHCl_3$); ^{1}H NMR (400 MHz, acetone-d_6) δ 10.07 (br s, 1H), 7.88 (br d, *J* = 8.6 Hz, 2H), 7.59 (br d, *J* = 7.8 Hz, 1H), 7.51 (br d, *J* = 7.8 Hz, 2H), 7.45 (d, *J* = 7.8 Hz, 3H), 7.37-7.26 (m, 4H), 7.17-7.04 (m, 3H), 6.98 (t, *J* = 7.4 Hz, 1H), 6.90 (br d, *J* = 7.4 Hz, 1H), 6.16-6.07 (m, 2H), 5.72 (dd, *J* = 8.6, 5.9 Hz, 1H), 5.21 (br s, 2H), 5.11 (br s, 1H), 4.69 (q, *J* = 7.0 Hz, 1H), 3.56 (s, 3H), 3.13 (t, *J* = 14.5 Hz, 1H), 3.00 (t, *J* = 14.5 Hz, 1H), 2.92-2.74 (m, 4H), 2.52-2.44 (m, 1H), 2.30 (s, 3H), 1.33 (br s, 9H), 0.75 (br d, *J* = 7.0 Hz, 3H); ^{13}C NMR (101 MHz, acetone-d_6) δ 172.5, 172.5, 171.4, 170.6, 170.6, 165.9, 155.8, 148.8, 146.0, 137.6, 137.3, 136.2, 130.9, 129.5, 128.7, 128.1, 128.0, 126.8, 126.0, 124.4, 128.0, 124.0, 123.6, 122.2, 119.6, 119.6, 114.9, 114.7, 113.2, 113.1, 113.1, 113.1, 112.2, 112.2, 112.2, 111.4, 79.3, 54.8, 52.7, 52.6, 51.9, 51.9, 50.7, 42.7, 42.5, 38.8, 38.1, 28.6, 29.5, 21.6, 15.4; HRMS (ESI) m/z calcd. for $C_{45}H_{51}F_3N_5O_8S$ $[M+H]^+$, 878.3410; found, 878.3417.

Methyl (6S,10S,13R,14S,E)-10-((1H-indol-3-yl)methyl)-6-(4-fluorophenyl)-2,2,14-trimethyl-4,8,11-trioxo-13-(1-tosyl-1H-pyrrol-2-yl)-3-oxa-5,9,12-triazaoctadec-15-en-18-oate (16i): 79% yield from **7b,** after deprotection and coupling to **14i**, according to the general procedure, part A. $[\alpha]^{25}_D$ +5 (*c* 0.28, $CHCl_3$); ^{1}H NMR (400 MHz, acetone-d_6) δ 10.06 (br s, 1H), 7.92 (d, *J* = 8.6 Hz, 2H), 7.62 (d, *J* = 7.8 Hz, 1H), 7.47-7.26 (m, 8H), 7.17 (dd, *J* = 3.1, 2.0 Hz, 1H), 7.14-7.08 (m, 2H), 7.01 (t, *J* = 7.2 Hz, 1H), 6.95 (br t, *J* = 8.8 Hz, 1H), 6.89-6.76 (m, 1H), 6.16 (br t, *J* = 3.3 Hz, 1H), 6.13 (br s, 1H), 5.75 (dd, *J* = 8.8, 5.7 Hz, 1H), 5.27-5.21 (m, 2H), 5.06 (br s, 1H), 4.71 (dd, *J* = 14.5, 7.3 Hz, 1H), 3.60 (s, 3H), 3.16 (dd, *J* = 14.5, 7.0 Hz, 1H), 3.02 (dd, J = 14.0, 7.0 Hz, 1H), 2.86 (br d, *J* = 2.3 Hz, 2H), 2.82-2.72 (m, 1H), 2.68-2.59 (m, 1H), 2.51 (br dd, J=6.50, 11.00 Hz, 1H), 2.35 (s, 3H), 1.36 (br s, 9H), 0.79 (d, *J* = 7.0 Hz, 3H);

^{13}C NMR (101 MHz, acetone-d_6) δ 172.5, 171.4, 170.8, 163.9, 161.4, 155.8, 146.1, 137.6, 137.3, 136.3, 136.2, 130.9, 129.2, 129.1, 128.7, 128.1, 124.5, 124.4, 124.0, 123.6, 122.3, 119.7, 119.6, 115.8, 115.6, 115.2, 114.9, 113.1, 112.3, 111.4, 79.2, 79.1, 54.8, 52.3, 51.9, 51.9, 50.7, 50.7, 43.1, 42.6, 38.2, 29.1, 28.7, 21.6, 15.4; HRMS (ESI) m/z calcd. for $C_{44}H_{51}FN_5O_8S$ $[M+H]^+$, 828.3442; found, 828.3446.

Methyl (6R,10S,13R,14S,E)-10-((1H-indol-3-yl)methyl)-6-(4-chlorobenzyl)-2,2,14-trimethyl-4,8,11-trioxo-13-(1-tosyl-1H-pyrrol-2-yl)-3-oxa-5,9,12-triazaoctadec-15-en-18-oate (16k): 80% yield from **7b,** after deprotection and coupling to **14k**, according to the general procedure, part A. ^{1}H NMR (500 MHz, acetone-d_6) δ 10.06 (br s, 1H), 7.93 (d, *J* = 8.3 Hz, 2H), 7.67 (d, *J* = 7.83 Hz, 1H), 7.39-7.35 (m, 4H), 7.22 (s, 1H), 7.19-7.14 (m, 3H), 7.12-7.08 (m, 1H), 7.00-7.05 (m, 2H), 7.05-7.03 (m, 1H), 6.24 (dd, *J* = 3.4, 1.5 Hz, 1H), 6.17 (t, *J* = 3.4 Hz, 1H), 6.13 (br d, *J* = 8.8 Hz, 1H), 5.79 (dd, *J* = 8.8, 5.9 Hz, 1H), 5.37-5.31 (m, 2H), 4.83 (q, *J* = 7.5 Hz, 1H), 4.07-3.98 (m, 1H), 3.60 (s, 3H), 3.28 (dd, *J* = 14.9, 6.4 Hz, 1H), 3.11 (dd, *J* = 14.9, 7.6 Hz, 1H), 2.89 (br d, *J* = 4.4 Hz, 2H), 2.82 (s, 1H), 2.67-2.59 (m, 3H), 2.37 (dd, *J* = 6.3, 3.3 Hz, 2H), 2.35 (s, 3H), 1.33 (s, 9H), 0.85 (d, *J* = 7.3 Hz, 3H); ^{13}C NMR (126 MHz, acetone-d_6) δ 172.5, 171.7, 171.5, 156.0, 146.0, 138.8, 137.7, 137.3, 136.4, 136.3, 132.2, 132.0 (2C), 130.9 (2C), 129.0 (2C), 128.8, 128.8, 128.1 (2C), 124.4, 124.0, 123.7, 122.3, 119.7, 119.6, 114.9, 113.1, 112.3, 111.6, 78.8, 54.6, 51.9, 51.9, 50.8, 42.7, 40.5, 40.2, 38.2, 29.0, 28.7, 21.6, 15.5; HRMS (ESI) m/z calcd. for $C_{45}H_{52}ClN_5O_8SNa$ $[M+Na]^+$, 880.3123; found, 880.3133.

(3*S*,14*S*,15*R*,*E*)-3-((1*H*-indol-3-yl)methyl)-14-methyl-15-(1-tosyl-1*H*-pyrrol-2-yl)-1,4,9-triazacyclopentadec-12-ene-2,5,10-trione (17): 29% yield from **16a** according to the general procedure, part B. ^{1}H NMR (400 MHz, acetone-d_6) δ 10.02 (br s, 1H), 7.92 (d, *J* = 8.2 Hz, 2H), 7.61 (d, *J* =7.8 Hz, 1H), 7.40 (d, *J* = 8.2 Hz, 2H), 7.36 (d, *J* = 8.2 Hz, 1H), 7.30 (q, *J* = 1.5 Hz, 1H), 7.12 (s, 1H), 7.11-6.98 (m, 5H), 6.62 (q, *J* = 1.5 Hz, 1H), 6.28 (t, *J* = 3.3 Hz, 1H), 5.96 (dd, *J* = 9.0, 4.3 Hz, 1H), 5.48-5.30 (m, 2H), 4.63 (ddd, *J* = 10.9, 7.7, 3.2 Hz, 1H), 3.48 (dd, *J* = 14.9, 3.1 Hz, 1H), 3.44-3.32 (m, 1H), 2.97-2.87 (m, 1H), 2.83 (br d, *J* = 6.6 Hz, 2H), 2.75-2.62 (m, 1H), 2.72 (br d, *J* = 8.6 Hz, 1H), 2.38 (s, 3H), 2.34-

2.23 (m, 1H), 2.13-2.06 (m, 1H), 1.87 (q, *J* = 12.5 Hz, 1H), 1.50-1.38 (m, 1H), 0.90 (d, *J* = 7.0 Hz, 3H); ^{13}C NMR (101 MHz, acetone-d_6) δ 174.4, 171.8, 171.3, 146.2, 137.7, 137.3, 136.2, 134.2, 131.0 (2 C), 128.7, 128.2 (2 C), 127.1, 124.1, 123.5, 122.2, 119.7, 119.2, 116.2, 113.1, 112.3, 112.3, 56.0, 49.8, 41.5, 41.2, 41.1, 35.1, 28.7, 23.9, 21.6, 16.7; HRMS (ESI) m/z calcd. for $C_{33}H_{37}N_5O_5SNa$ $[M+Na]^+$, 638.2413; found, 638.2415.

(3*S*,15*S*,16*R*,*E*)-3-((1*H*-indol-3-yl)methyl)-15-methyl-16-(1-tosyl-1*H*-pyrrol-2-yl)-1,4,10-triazacyclohexadec-13-ene-2,5,11-trione (18): 22% yield from **16b** according to the general procedure, part B. $[\alpha]^{25}_D$ +49 (*c* 0.11, $CHCl_3$); ^{1}H NMR (400 MHz, acetone-d_6) δ 9.99 (br s, 1H), 8.02 (d, *J* = 8.2 Hz, 2H), 7.55 (d, *J* = 7.8 Hz, 1H), 7.40 (d, *J* = 8.2 Hz, 2H), 7.36 (d, *J* = 8.2 Hz, 2H) 7.25 (br d, *J* = 1.6 Hz, 1H), 7.21 (br d, *J* = 7.8 Hz, 1H), 7.14-7.05 (m, 2H), 7.03 (s, 1H), 6.97 (t, *J* =7.4 Hz, 1H), 6.44 (br s, 1H), 6.25 (br s, 1H0, 6.04 (dd, *J* = 8.4, 3.3 Hz, 1H), 5.51 (ddd, *J* = 15.6, 7.8, 5.5 Hz, 1H), 5.41 (dd, *J* = 15.6, 7.8 Hz, 1H), 4.71-4.64 (m, 1H), 3.69-3.54 (m, 1H), 3.33-3.23 (m, 2H), 3.03-2.81 (m, 3H), 1.98-1.84 (m, 2H), 1.68-1.49 (m, 4H), 2.34 (s, 3H), 0.94 (d, , *J* = 6.6 Hz, 3H); ^{13}C NMR (101 MHz, acetone-d_6) δ 174.3, 171.9, 171.6, 146.1, 137.6, 137.4, 135.7, 135.1, 130.9 (2 C), 128.7, 128.4 (2 C), 126.7, 124.1, 123.8, 122.2, 119.6, 119.2, 116.0, 113.3, 112.3, 111.9, 55.8, 49.7, 41.9, 41.2, 37.1, 34.3, 30.7, 28.7, 28.6, 21.6, 16.7; HRMS (ESI) m/z calcd. for $C_{34}H_{39}N_5O_5SNa$ $[M+Na]^+$, 652.2570; found, 652.2565.

(3*S*,13*S*,14*R*,*E*)-3-((1*H*-Indol-3-yl)methyl)-13-methyl-14-(1-tosyl-1*H*-pyrrol-2-yl)-1,4,8-triazacyclotetradec-11-ene-2,5,9-trione (19): 41% yield from **16c** according to the general procedure, part B. $[\alpha]^{25}_D$ +5 (*c* 0.193, $CHCl_3$); ^{1}H NMR (400 MHz, acetone-d_6) δ 10.02 (br s, 1H), 8.03 (d, *J* = 8.2 Hz, 2H), 7.59-7.49 (m, 2H), 7.40 (d, *J* = 8.2 Hz, 2H), 7.35 (d, *J* = 8.2 Hz, 1H), 7.23 (d, *J* = 2.0 Hz, 1H), 7.08 (t, *J* = 7.1 Hz, 1H), 7.02 (s, 1H), 6.98 (t, *J* = 7.5 Hz, 1H), 6.89 (br d, *J* = 7.4 Hz, 1H), 6.26 (s, 2H), 5.86 (dd, *J* = 7.4, 3.9 Hz, 1H), 5.71-5.56 (m, 2H), 4.69 (t, *J* = 8.1 Hz, 1H), 3.51-3.40 (m, 1H), 3.23 (dd, *J* = 14.9, 3.9 Hz, 1H), 3.19-3.10 (m, 1H), 3.08-2.96 (m, 2H), 2.94-2.84 (m, 1H), 2.83-2.68 (m, 2H), 2.54 (tt, *J* = 11.4, 4.1 Hz, 1H), 2.36 (s, 3H), 0.90 (d, *J* = 7.0 Hz, 3H); ^{13}C NMR (101 MHz, acetone-d_6) δ 172.0,

171.8, 171.5, 146.1, 137.6, 137.4, 135.8, 135.0, 130.9, 128.6, 128.2, 127.7, 124.1, 123.8, 122.2, 119.6, 119.1, 115.1, 113.4, 112.3, 111.6, 56.3, 50.2, 42.3, 41.2, 36.0, 35.5, 28.6, 21.6, 14.8; HRMS (ESI) m/z calcd. for $C_{32}H_{35}N_5O_5SNa$ $[M+Na]^+$, 624.2257; found, 624.2268.

(3*S*,7*S*,13*S*,14*R*,*E*)-3-((1*H*-indol-3-yl)methyl)-13-methyl-7-phenethyl-14-(1-tosyl-1*H*-pyrrol-2-yl)-1,4,8-triazacyclotetradec-11-ene-2,5,9-trione (20): 70% overall yield from **7b/14d** according to the general procedures, parts A and B; $[\alpha]^{25}_D$ = +13 (*c* 0.11, $CHCl_3$); ^{1}H NMR (400 MHz, acetone-d_6) δ 10.00 (br s, 1H), 7.99 (d, *J* = 8.4 Hz, 2H), 7.60 (br d, *J* = 8.6 Hz, 1H), 7.53 (d, *J* = 8.0 Hz, 1H), 7.40 (br d, *J* = 8.4 Hz, 2H), 7.36 (d, *J* = 8.0 Hz, 1H), 7.28-7.31 (m, 1H), 7.14-7.27 (m, 6H), 7.08 (t, *J* = 8.0 Hz, 1H), 7.03 (s, 1H), 6.98 (t, *J* = 8.0 Hz, 1H), 6.86 (br d, *J* = 8.6 Hz, 1H), 6.31 (br s, 1H), 6.30-6.28 (m, 1H), 5.99 (dd, *J* = 8.6, 3.5 Hz, 1H), 5.59 (ddd, *J* = 15.8, 8.2, 5.0 Hz, 1H), 5.51 (dd, *J* = 15.8, 7.4 Hz, 1H), 4.74 (ddd, *J* = 10.2, 8.6, 3.0 Hz, 1H), 4.12-4.25 (m, 1H), 3.34 (dd, *J* = 14.8, 3.5 Hz, 1H), 2.84-2.92 (m, H_2O overlap), 2.50-2.70 (m, 6H), 2.35 (s, 3H), 2.24 (dd, *J* = 15.2, 3.5 Hz, 1H), 1.81-1.93 (m, 1H), 1.65-1.77 (m, 1H), 0.85 (d, *J* = 6.6 Hz, 3H); ^{13}C NMR (100 MHz, acetone-d_6) δ 171.4, 171.2, 170.6, 145.6, 142.4, 137.0, 136.6, 134.1, 133.5, 130.3, 128.7, 128.6, 128.0, 127.7, 126.0, 123.4, 123.2, 121.6, 119.1, 118.5, 55.0, 48.5, 47.3, 42.2, 41.5, 41.0, 36.8, 32.7, 28.0, 21.0, 15.6; HRMS (ESI) m/z calcd for $C_{40}H_{44}N_5O_5S$ $[M+H]^+$, 706.3063; found, 706.3052.

(3*S*,7*R*,13*S*,14*R*,*E*)-3-((1*H*-Indol-3-yl)methyl)-13-methyl-7-phenethyl-14-(1-tosyl-1*H*-pyrrol-2-yl)-1,4,8-triazacyclotetradec-11-ene-2,5,9-trione (21): 39% overall yield from **7b/14e** according to the general procedures; $[\alpha]^{25}_D$ +57 (*c* 0.10, $CHCl_3$); ^{1}H NMR (400 MHz, acetone-d_6) δ 10.00 (br s, 1H), 7.98 (d, *J* = 8.2 Hz, 2H), 7.55 (d, *J* = 7.8 Hz, 1H), 7.34-7.41 (m, 3H), 7.22-7.32 (m, 4H), 7.14-7.20 (m, 3H), 7.09 (br t, *J* = 8.0 Hz, 2 H), 6.97-7.04 (m, 2H), 6.87 (br d, *J* = 8.6 Hz, 1H), 6.50 (br s, 1H), 6.31 (t, *J* = 3.5 Hz, 1H), 5.99 (dd, *J* = 8.6, 3.5 Hz, 1H), 5.60 (ddd, *J* = 14.9, 7.8, 6.3 Hz,

1H), 5.49 (dd, *J* = 14.9, 7.4 Hz, 1H), 4.56 (ddd, *J* = 11.0, 8.2, 3.5 Hz, 1H), 4.07-4.18 (m, 1H), 3.23 (dd, *J* = 14.8, 3.5 Hz, 1H), 3.05 (dd, *J* = 12.1, 5.9 Hz, 1H), 2.69-2.77 (m, 2H), 2.52-2.68 (m, 4H), 2.31 (s, 3H), 2.14 (dd, *J* = 14.8, 7.8 Hz, 1H), 1.93-2.02 (m, 1H), 1.72-1.83 (m, 1H), 0.93 (d, *J* = 7.0 Hz, 3H); ^{13}C NMR (100 MHz, acetone-d_6) δ 171.3, 171.1, 170.9, 145.5, 142.4, 137.0, 136.7, 134.7, 134.2, 130.3, 128.7, 128.6, 128.0, 127.6, 127.1, 126.0, 123.5, 123.1, 121.6, 119.0, 118.5, 115.5, 112.8, 111.7, 111.1, 56.4, 49.1, 46.6, 41.6, 41.2, 40.7, 36.9, 32.8, 28.0, 20.9, 15.5; HRMS (ESI) m/z calcd. for $C_{40}H_{44}N_5O_5S$ $[M+H]^+$, 706.3063; found, 706.3029.

(3*S*,7*S*,13*S*,14*R*,*E*)-3-((1*H*-Indol-3-yl)methyl)-13-methyl-14-(1-tosyl-1*H*-pyrrol-2-yl)-7-(3-(trifluoromethyl)phenyl)-1,4,8-triazacyclotetradec-11-ene-2,5,9-trione (22): 28% overall yield from **7b/14f** according to the general procedures, parts A and B. $[\alpha]^{25}_D$ +27 (*c* 0.19, $CHCl_3$); ^{1}H NMR (500 MHz, acetone-d_6) δ 10.01 (br s, 1H), 7.94 (d, *J* = 8.4 Hz, 2H), 7.82 (d, *J* = 8.6 Hz, 1H), 7.72 (s, 1H), 7.67 (d, *J* = 7.4 Hz, 1H), 7.61-7.54 (m, 3H), 7.49 (d, *J* = 7.0 Hz, 1H), 7.39 (d, *J* = 8.4 Hz, 2H), 7.36 (d, *J* = 7.8 Hz, 1H), 7.33 (dd, *J* = 3.1, 1.6 Hz, 1H), 7.13-6.99 (m, 4H), 6.54 (dd, *J* = 3.1, 1.6 Hz, 1H), 6.34 (t, *J* = 3.1 Hz, 1H), 6.03 (dd, *J* = 8.6, 4.3 Hz, 1H), 5.70-5.47 (m, 3H), 4.45 (ddd, *J* = 10.9, 7.4, 5.3 Hz, 1H), 3.26 (dd, *J* = 14.9, 3.5 Hz, 1H), 3.10 (dd, *J* = 11.9, 6.0 Hz, 1H), 2.99 (dd, *J* = 14.9, 10.9 Hz, 1H), 2.77-2.70 (m, 2H), 2.65-2.60 (m, 1H), 2.52 (dd, *J* = 14.5, 10.9, 1H), 2.29 (s, 3H), 0.95 (d, *J* = 7.0 Hz, 3H); ^{13}C NMR (101 MHz, acetone-d_6) δ 171.1, 171.0, 170.6, 145.6, 144.4, 137.1, 136.7, 135.3, 133.7, 130.7, 130.3, 130.2 (q, $^2J_{C\text{-}F}$ = 70.0 Hz), 129.7, 127.9, 127.6, 126.9 (q, $^1J_{C\text{-}F}$ = 262.3 Hz), 126.5, 124.1 (q, $^3J_{C\text{-}F}$ = 3.9 Hz), 123.6, 123.4 (q, $^3J_{C\text{-}F}$ = 3.9 Hz), 123.1, 121.7, 119.1, 118.5, 115.8, 112.8, 111.8, 111.2, 57.5, 50.1, 49.2, 43.4, 41.4, 41.2, 27.8, 20.9, 16.2; HRMS (ESI) m/z calcd. for $C_{39}H_{39}F_3N_5O_5S$ $[M+H]^+$, 746.2624; found, 746.2642.

(3*S*,7*S*,13*S*,14*R*,*E*)-3-((1*H*-Indol-3-yl)methyl)-13-methyl-14-(1-tosyl-1*H*-pyrrol-2-yl)-7-(4-(trifluoromethyl)phenyl)-1,4,8-triazacyclotetradec-11-ene-2,5,9-trione (23): 46% yield from **16g**

according to the general procedure, part B. $[\alpha]^{25}_{D}$ +38 (*c* 0.36, $CHCl_3$); ^{1}H NMR (500 MHz, acetone-d_6) δ 9.99 (br s, 1H), 7.94 (d, *J* = 8.4 Hz, 2H), 7.75 (d, *J* = 8.5 Hz, 1H), 7.64 (d, *J* = 7.6 Hz, 2H), 7.60-7.56 (m, 3H), 7.49 (br d, *J* = 7.3 Hz, 1H), 7.39 (d, *J* = 7.9 Hz, 2H), 7.36 (d, *J* = 8.0 Hz, 1H), 7.32 (dd, *J* = 3.4, 1.7 Hz, 1H), 7.10 (ddd, *J* = 8.0, 6.9, 1.2 Hz, 1H), 7.07 (s, 1H), 7.03 (dt, *J* = 1.1, 7.4 Hz, 2H), 6.53 (dd, *J* = 3.4, 1.5 Hz, 1H), 6.34 (t, *J* = 3.4 Hz, 1H), 6.02 (dd, *J* = 8.7, 4.1 Hz, 1H), 5.64 (ddd, *J* = 15.4, 8.8, 6.0 Hz, 1H), 5.48-5.57 (m, 2H), 4.44 (ddd, *J* = 11.0, 7.6, 3.7 Hz, 1H), 3.25 (dd, *J* = 15.0, 3.6 Hz, 1H), 3.11 (dd, *J* = 11.9, 6.1 Hz, 1H), 2.96 (dd, *J* = 14.5, 10.7 Hz, 1H), 2.81-2.79 (m, 1H), 2.77-2.71 (m, 5H), 2.66-2.58 (m, 1H), 2.51 (dd, *J* = 14.5, 10.8 Hz, 1H), 0.95 (d, *J* = 7.0 Hz, 3H); ^{13}C NMR (126 MHz, acetone-d_6) δ 171.7, 171.6, 171.2, 148.1, 146.2, 137.7, 137.3, 135.8, 134.3, 130.9 (2 C), 129.5 (q, $^2J_{C\text{-}F}$ = 32.2 Hz, C), 128.5, 128.2 (2 C), 128.0 (2 C), 127.1, 126.2 (q, $_{3J/C\text{-}F}$ = 3.6 Hz, 2 C), 127.5 (q, $^1J_{C\text{-}F}$ = 259 Hz, CF_3), 124.2, 123.7, 122.4, 119.7, 119.1, 116.4, 113.3, 112.4, 111.9, 58.1, 50.6, 49.8, 43.8, 41.9, 41.7, 28.3, 21.5, 16.7; HRMS (ESI) m/z calcd. for $C_{39}H_{38}F_3N_5O_5SNa$ $[M+Na]^+$, 768.2443; found, 768.2479.

(3*S*,7*S*,13*S*,14*R*,*E*)-3-((1*H*-indol-3-yl)methyl)-13-methyl-7-(*p*-tolyl)-14-(1-tosyl-1*H*-pyrrol-2-yl)-1,4,8-triazacyclotetradec-11-ene-2,5,9-trione (24): 26% overall yield from **7b/14h** according to the general procedures, parts A and B. $[\alpha]^{25}_{D}$ +40 (*c* 0.166, $CHCl_3$); ^{1}H NMR (400 MHz, acetone-d_6) δ 10.01 (br s, 1H), 7.94 (d, *J* = 8.2 Hz, 2H), 7.70 (d, *J* = 9.0 Hz, 1H), 7.59 (d, *J* = 8.2 Hz, 1H), 7.42 (d, *J* = 7.4 Hz, 1H), 7.40-7.34 (m, 3H), 7.33 (d, *J* = 3.5, 1.6 Hz, 1H), 7.22 (d, *J* = 8.2 Hz, 2H), 7.12-6.97 (m, 6H), 6.63 (dd, *J* = 3.1, 1.6 Hz, 1H), 6.34 (dd, *J* = 3.1, 3.5 Hz, 1H), 6.07 (dd, *J* = 9.0, 4.3 Hz, 1H), 5.60 (ddd, *J* = 15.4, 9.4, 5.3 Hz, 1H), 5.47 (dd, *J* = 15.4, 8.6 Hz, 1H), 5.49-5.40 (m, 1H), 4.45 (ddd, *J* = 10.8, 7.5, 3.4 Hz, 1H), 3.26 (dd, *J* = 14.7, 3.4 Hz, 1H), 3.06 (dd, *J* = 11.7, 5.3 Hz, 1H), 2.92 (dd, *J* = 14.7, 10.8 Hz, 1H), 2.69 (dd, *J* = 11.7, 9.4 Hz, 1H), 2.63 (dd, *J* = 14.5, 4.5 Hz, 1H), 2.60-2.50 (m, 1H), 2.41 (dd, *J* = 14.3, 11.5 Hz, 1H). 2.28 (s, 3H), 2.26 (s, 3H), 0.96 (d, *J* = 6.6 Hz, 3H); ^{1}H NMR (101 MHz, acetone-d_6) δ 171.0, 170.5, 170.2, 145.2, 139.5, 136.7, 136.3 (2C), 134.7, 133.1, 130.0, 128.9, 127.6, 127.2, 126.4, 126.1, 123.3, 122.7, 121.3, 118.7, 118.1, 115.7, 112.4, 111.4, 110.0, 57.1, 49.5, 48.6, 43.8, 41.1, 40.9, 27.5, 20.6, 20.1, 16.1; HRMS (ESI) m/z calcd. for $C_{39}H_{42}N_5O_5S$ $[M+H]^+$, 692.2907; found, 692.2915.

(3*S*,7*S*,13*S*,14*R*,*E*)-3-((1*H*-indol-3-yl)methyl)-7-(4-fluorophenyl)-13-methyl-14-(1-tosyl-1*H*-pyrrol-2-yl)-1,4,8-triazacyclotetradec-11-ene-2,5,9-trione (25): 42% yield from **16i** according to the general procedure, part B. $[\alpha]^{25}_{D}$ +17 (*c* 0.146, $CHCl_3$); ^{1}H NMR (400 MHz, acetone-d_6) δ 10.01 (br s, 1H), 7.94 (d, *J* = 8.2 Hz, 2H), 7.71 (br d, *J* = 8.6 Hz, 1H), 7.58 (d, *J* = 7.8 Hz, 1H), 7.44 (br d, *J* = 7.0 Hz, 1H), 7.42-7.34 (m, 5H), 7.33 (dd, *J* = 3.1, 1.6 Hz, 1H), 7.13-6.97 (m, 6H), 6.58 (d, *J* = 1.6 Hz, 1H), 6.34 (t, *J* = 3.3 Hz, 1H), 6.04 (dd, *J* = 8.7, 3.9 Hz, 1H), 5.66-5.56 (m, 1H), 5.53-5.42 (m, 2H), 4.44 (s, 1H), 3.26 (dd, *J* = 14.5, 3.1 Hz, 1H), 3.06 (dd, *J* = 11.7, 5.5 Hz, 1H), 2.96-2.88 (m, 1H), 2.74-2.64 (m, 2H), 2.62-2.55 (m, 1H), 2.45 (dd, *J* = 14.1, 11.3 Hz, 1H), 2.29 (s, 3H), 0.95 (d, *J* = 7.0 Hz, 3H); ^{13}C NMR (101 MHz, acetone-d_6) δ 171.8, 171.5, 171.1, 162.7 (d, $^1J_{C\text{-}F}$ = 258.3 Hz, 2C), 146.1, 139.7, 137.7, 137.3, 135.7, 134.2, 130.9 (2C), 129.1, 129.2, 128.5, 128.2 (2C), 127.2, 124.2, 123.7, 122.3, 119.7, 119.1, 116.6, 115.8 (d, $^2J_{C\text{-}F}$ = 21.7 Hz, 2C), 113.3, 112.4, 112.3, 111.9, 58.0, 50.2, 49.7, 44.3, 42.0, 41.8, 30.9, 30.7, 28.4, 21.5, 16.9; HRMS (ESI) m/z calcd. for $C_{38}H_{38}FN_5O_5SNa$ $[M+Na]^+$, 718.2475; found, 718.2488.

(3*S*,7*S*,13*S*,14*R*,*E*)-3-((1*H*-indol-3-yl)methyl)-7-(4-chlorophenyl)-13-methyl-14-(1-tosyl-1*H*-pyrrol-2-yl)-1,4,8-triazacyclotetradec-11-ene-2,5,9-trione (26): 36% overall yield from **7b/14j**, according to the general procedures, parts A and B. $[\alpha]^{25}_{D}$ +33 (*c* 0.14, $CHCl_3$); ^{1}H NMR (400 MHz, acetone-d_6) δ 10.03 (br s, 1H), 7.94 (d, *J* = 8.2 Hz, 2H), 7.75 (d, *J* = 8.6 Hz, 1H), 7.58 (d, *J* = 7.8 Hz, 1H), 7.49 (d, *J* = 7.4 Hz, 1H), 7.43-7.30 (m, 8H), 7.14-7.00 (m, 4H), 6.56 (br s, 1H), 6.33 (t, *J* = 3.1 Hz, 1H), 6.03 (dd, *J* = 8.6, 3.9 Hz, 1H), 5.62 (ddd, *J* = 14.9, 8.2, 6.1 Hz, 1H), 5.50 (dd, *J* = 14.9, 8.6 Hz, 1H), 5.50-5.40 (m, 1H), 4.44 (ddd, *J* = 10.8, 7.8, 2.9 Hz, 1H), 3.25 (d, *J* = 14.9, 2.9 Hz, 1H), 3.08 (dd, *J* = 11.9, 6.1 Hz, 1H), 2.94 (dd, *J* = 14.9, 10.8 Hz, 1H), 2.71 (dd, *J* = 11.9, 8.2 Hz, 1H), 2.68 (dd, *J* = 14.1, 4.5 Hz, 1H), 2.63-2.56 (m, 1H), 2.46 (dd, *J* = 14.1, 11.3 Hz, 1H), 2.29 (s, 3H), 0.95 (d, *J* = 6.6 Hz, 3H); ^{13}C NMR (100 MHz, acetone-d_6) δ 170.8, 170.6, 170.2, 145.2, 141.5, 136.7, 136.3, 134.8, 133.2, 132.1, 130.0, 128.3, 128.1, 127.5, 127.2, 126.2, 123.3, 122.7, 121.4, 118.7, 118.1, 115.5, 112.4, 111.4, 110.9, 57.1, 49.3, 48.8, 43.1, 41.0, 40.8, 27.4, 20.6, 15.9; HRMS (ESI) m/z calcd. for $C_{38}H_{39}ClN_5O_5S$ $[M+H]^+$, 712.2360; found, 712.2380.

(3*S*,7*R*,13*S*,14*R*,*E*)-3-((1*H*-indol-3-yl)methyl)-7-(4-chlorobenzyl)-13-methyl-14-(1-tosyl-1*H*-pyrrol-2-yl)-1,4,8-triazacyclotetradec-11-ene-2,5,9-trione (27): 42% yield from **16k** according to the general procedure, part B. $[\alpha]^{25}_{D}$ +57 (*c* 0.22, $CHCl_3$); ^{1}H NMR (400 MHz, acetone-d_6) δ 9.98 (br s, 1H), 7.98 (d, *J* = 8.3 Hz, 2H), 7.53 (d, *J* = 7.8 Hz, 1H), 7.41-7.36 (m, 3H), 7.33 (br d, *J* = 7.8 Hz, 1H), 7.28-7.24 (m, 3H), 7.20 (d, *J* = 8.8 Hz, 2H), 7.09 (t, *J* = 7.6 Hz, 2H), 7.00-6.95 (m, 2H), 6.87 (br d, *J* = 7.8 Hz, 1H), 6.42 (dd, *J* = 3.2, 1.7 Hz, 1H), 6.29 (t, *J* = 3.2 Hz, 1H), 5.96 (dd, *J* = 8.6, 4.2 Hz, 1H), 5.59 (ddd, *J* = 15.2, 8.8, 6.7 Hz, 1H), 5.49 (dd, *J* = 15.2, 8.3 Hz, 1H), 4.59 (ddd, *J* = 10.4, 8.0, 3.7 Hz, 1H), 4.29 (dddd, *J* = 15.2, 8.5, 7.3, 4.9 Hz, 1H), 3.23 (dd, *J* = 14.9, 23.7 Hz, 1H), 3.01-2.87 (m, 5H), 2.64 (dd, *J* = 12.2, 8.5 Hz, 1H), 2.51 (dd, *J* = 15.0, 4.9 Hz, 1H), 2.32 (s, 3H), 2.12 (dd, *J* = 15.0, 7.3 Hz, 1H), 0.91 (d, *J* = 7.3 Hz, 3H); ^{13}C NMR (101 MHz, acetone-d_6) δ 172.3, 172.0, 172.0, 146.6, 139.4, 138.2, 137.9, 135.9, 135.4, 133.0, 132.5, 131.4, 129.7, 129.7, 129.6, 129.1, 12.7, 128.1, 124.6, 124.3, 122.8, 120.2, 119.6, 116.5, 113.9, 112.8, 112.8, 112.3, 57.5, 50.3, 49.4, 42.6, 42.3, 40.9, 40.5, 29.1, 22.0, 16.6; HRMS (ESI) m/z calcd. for $C_{39}H_{43}ClN_5O_5S$ $[M+H]^+$, 726.2517; found, 726.2508.

(3*S*,7*S*,13*S*,14*R*,*E*)-3-((1*H*-indol-3-yl)methyl)-13-methyl-14-phenyl-7-(4-(trifluoromethyl)phenyl)-1,4,8-triazacyclotetradec-11-ene-2,5,9-trione (28): 19% overall yield from **7a/14g,** according to the general procedures part A and B. $[\alpha]^{25}_{D}$ = +10 (*c* 0.35, $CHCl_3$); ^{1}H NMR (400 MHz, acetone-d_6) δ 9.99 (br s, 1H), 7.92 (s, 1H), 7.80 (br d, *J* = 8.2 Hz, 1H), 7.67-7.55 (m, 5H), 7.52 (d, *J* = 7.8 Hz, 1H), 7.34-7.27 (m, 5H), 7.27-7.20 (m, 1H), 7.07 (s, 1H), 7.04 (t, *J* = 7.4 Hz, 1H), 6.95 (t, *J* = 7.4 Hz, 1H), 5.75 (ddd, *J* = 15.3, 9.1, 6.5 Hz, 1H), 5.59-5.49 (m, 1H), 5.29 (dd, *J* = 15.3, 9.4 Hz, 1H), 4.95 (dd, *J* = 8.4, 4.1 Hz, 1H), 4.53-4.44 (m, 1H), 3.33 (dd, *J* = 15.0, 4.4 Hz, 1H), 3.14 (dd, *J* = 15.0, 10.6 Hz, 1H), 3.10-3.05 (m, 1H), 2.80-2.75 (m, 1H), 2.68 (dd, *J* = 11.9, 9.6 Hz, 1H), 2.62-2.49 (m, 2H), 0.85 (d, *J* = 7.0 Hz, 3H); ^{13}C NMR (101 MHz, acetone-d_6) δ 171.7, 171.5, 171.1, 148.2, 139.8, 137.7, 135.7, 129.4 (2 C), 129.5 (q, $^2J_{C\text{-}F}$ = 32.3 Hz, 1 C), 128.7 (2 C), 128.6, 128.0 (2 C), 127.9, 127.2, 126.2 (q, $^3J_{C\text{-}F}$ = 3.8 Hz, 2C), 124.3, 122.2,

125.4 (q, $^{1}J_{C\text{-}F}$ = 271.7 Hz, 1 C), 119.7, 119.2, 112.3, 112.3, 112.0, 58.5, 57.8, 50.6, 43.7, 42.4, 41.6, 27.6, 17.6; HRMS (ESI) m/z calcd. for $C_{34}H_{44}F_3N_4O_3$ $[M+H]^+$, 603.2583; found, 603.2582.

(3*S*,7*S*,13*S*,14*R*,*E*)-3-((1*H*-indol-3-yl)methyl)-7-(4-fluorophenyl)-13-methyl-14-phenyl-1,4,8-triazacyclotetradec-11-ene-2,5,9-trione (29): 33% yield from **15i** according to the general procedure, part B. $[\alpha]^{25}_{D}$ +15 (*c* 0.133, $CHCl_3$); ^{1}H NMR (500 MHz, acetone-d_6) δ 9.97 (br s, 1H), 7.69 (br d, *J* = 8.0 Hz, 1H), 7.55-7.54 (m, 1H), 7.56 (br d, *J* = 7.8 Hz, 1H), 7.43 (d, *J* = 5.3 Hz, 1H), 7.41 (d, *J* = 5.3 Hz, 1H), 7.36-7.31 (m, 6H), 7.31-7.25 (m, 2H), 7.11-7.09 (m, 2H), 7.09 (d, *J* = 5.3 Hz, 1H), 7.07 (s, 1H), 7.06-7.04 (m, 1H), 6.99 (t, *J* = 8.0 Hz, 1H), 5.76 (ddd, *J* = 15.2, 9.8, 6.1 Hz, 1H), 5.49 (dddd, *J* =12.2, 8.1, 3.7, 0.4 Hz, 1H), 5.30 (dd, *J* = 15.2, 9.8 Hz, 1H), 4.98 (dd, *J* = 8.3, 3.9 Hz, 1H), 4.52 (ddd, *J* = 10.2, 7.5, 3.9 Hz, 1H), 3.36 (dd, *J* = 14.9, 3.9 Hz, 1H), 3.15 (dd, *J* = 14.9, 10.2 Hz, 1H), 3.08 (dd, *J* = 12.2, 5.9 Hz, 1H), 2.76 (d, *J* = 4.4 Hz, 1H), 2.74 (dd, *J* = 14.9, 3.9 Hz, 1H), 2.77-2.72 (m, 1H), 2.74 (dd, *J* = 12.2, 5.9 Hz, 1H), 2.69 (dd, *J* = 12.2, 9.5 Hz, 1H), 2.58 (dd, *J* = 14.9, 3.7 Hz, 2H), 2.56-2.54 (m, 1H), 1.50-1.39 (m, 3H), 0.90 (d, *J* = 6.9 Hz, 3H); ^{13}C NMR (126 MHz, acetone-d_6) δ 171.9, 171.3, 171.0, 162.7 (d, $^{1}J_{C\text{-}F}$ = 243.4 Hz, 1 C), 139.8, 137.7, 135.6, 129.5 (2 C), 129.3, 129.2, 128.6 (2 C), 127.9 (2 C), 127.3, 124.3, 124.2, 122.2, 119.7, 119.2, 115.9 (d, $^{2}J_{C\text{-}F}$ = 21.1 Hz, 1C), 112.3, 112.0, 58.5, 57.7, 50.2, 44.3, 42.5, 41.7, 27.7, 17.8; HRMS (ESI) m/z calcd. for $C_{33}H_{34}FN_4O_3$ $[M+H]^+$, 553.2615; found, 553.2634.

(3*S*,7*S*,13*S*,14*R*,*E*)-3-((1*H*-indol-3-yl)methyl)-7-(4-chlorophenyl)-13-methyl-14-phenyl-1,4,8-triazacyclotetradec-11-ene-2,5,9-trione (30): 13% yield from **15j** according to the general procedure, part B. $[\alpha]^{25}_{D}$ +16 (*c* 0.146, $CHCl_3$); ^{1}H NMR (500 MHz, acetone-d_6) δ 9.97 (br s, 1H), 7.69 (br d, *J* = 8.8 Hz, 1H), 7.56 (d, *J* = 7.8 Hz, 2H), 7.41 (d, *J* = 8.3 Hz, 2H), 7.36-7.30 (m, 7H), 7.32-7.25 (m, 3H), 7.09 (d, *J* = 2.0 Hz, 1H), 7.07 (t, *J* = 7.8 Hz, 1H), 6.99 (t, *J* = 6.9 Hz, 1H), 5.76 (ddd, *J* = 15.3, 9.3, 5.9 Hz, 1H), 5.48 (ddd, *J* = 10.8, 8.8, 3.9 Hz, 1H), 5.31 (dd, *J* = 15.3, 9.6 Hz, 1H), 4.98 (dd, *J* = 8.3, 3.9 Hz, 1H), 4.52 (ddd, *J* = 10.2, 7.5, 3.9 Hz, 1H), 3.36 (dd, *J* = 14.9, 3.7 Hz, 1H), 3.15 (dd, *J* = 14.9, 10.0 Hz, 1H), 3.09 (dd, *J* = 11.9, 5.9 Hz, 1H), 2.76 (dd, *J* = 14.7, 3.9 Hz, 1H), 2.70 (dd, *J* = 11.9, 9.3 Hz, 1H), 2.57 (dd,

J = 14.7, 10.2 Hz, 1H), 2.60-2.52 (m, 1H), 0.90 (d, *J* = 6.9 Hz, 3H); ^{13}C NMR (126 MHz, acetone-d_6) δ 170.8, 170.3, 170.0, 141.6, 138.9, 136.7, 134.6, 132.1, 128.5, 128.3, 128.1, 127.7, 127.6, 126.9, 126.2, 123.3, 121.3, 118.7, 118.2, 111.3, 111.0, 57.5, 56.7, 49.3, 43.1, 41.5, 40.7, 26.7, 16.8; HRMS (ESI) m/z calcd. for $C_{33}H_{33}ClN_4O_3Na$ $[M+Na]^+$, 591.2139; found, 591.2147.

Abbreviations

EDCI, 1-ethyl-3-(3-dimethylaminopropyl)carbodiimide; (**HATU** (1-[Bis(dimethylamino)methylene]-1H-1,2,3-triazolo[4,5-b]pyridinium 3-oxid hexafluorophosphate, **H**exafluorophosphate **A**zabenzotriazole **T**etramethyl **U**ronium

Supporting Information Availability

Figure S1.

Coordinate files used to generate Figures 4 and 5.

Figure4-Dockingcoordinates-het.pdb

Figure5-Dockingcoordinates-het.pdb

Molecular Structures

jm-2018-01529y.csv

PDB ID codes

Coordinates have been deposited with the PDB with the following accession numbers: APE1 bound to DMSO (6MK3), DMSO/Mg^{2+} (6MKK), DMSO/Tris (6MKM), and GLC (6MKO). Authors will release the atomic coordinates and experimental data upon article publication.

Ancillary information

Corresponding authors Millie M. Georgiadis, mgeorgia@iu.edu; Mark R. Kelley, mkelley@iu.edu.

This work was supported by grants from the National Institutes of Health R01CA205166 to M.R.K., M.M.G. and R01CA167291 to M.R.K., as well as support provided by the Earl and Betty Herr Professor in Pediatric Oncology Research, Jeff Gordon Children's Foundation and the Riley Children's Foundation (M.R.K.).Work at the BU-CMD (J.A.P., Jr., L.E.B., R.T.) is supported by the National Institutes of

Health, R24 GM111625. D.B. and S.V. were supported by the National Institutes of Health, R35 GM118078. Present address Spandan Chennamadhavuni: Department of Chemistry, Emory University, Atlanta, GA 30322.

References

1. Shah, F.; Logsdon, D.; Messmann, R. A.; Fehrenbacher, J. C.; Fishel, M. L.; Kelley, M. R. Exploiting the Ref-1-APE1 node in cancer signaling and other diseases: from bench to clinic. *NPJ Precis Oncol* **2017**, 1-19.
2. Yuan, C. L.; He, F.; Ye, J. Z.; Wu, H. N.; Zhang, J. Y.; Liu, Z. H.; Li, Y. Q.; Luo, X. L.; Lin, Y.; Liang, R. APE1 overexpression is associated with poor survival in patients with solid tumors: a meta-analysis. *Oncotarget* **2017,** 8, 59720-59728.
3. Juhnke, M.; Heumann, A.; Chirico, V.; Hoflmayer, D.; Menz, A.; Hinsch, A.; Hube-Magg, C.; Kluth, M.; Lang, D. S.; Moller-Koop, C.; Sauter, G.; Simon, R.; Beyer, B.; Pompe, R.; Thederan, I.; Schlomm, T.; Luebke, A. M. Apurinic/apyrimidinic endonuclease 1 (APE1/Ref-1) overexpression is an independent prognostic marker in prostate cancer without TMPRSS2:ERG fusion. *Mol Carcinog* **2017,** 56, 2135-2145.
4. Chen, T.; Liu, C.; Lu, H.; Yin, M.; Shao, C.; Hu, X.; Wu, J.; Wang, Y. The expression of APE1 in triple-negative breast cancer and its effect on drug sensitivity of olaparib. *Tumour Biol* **2017,** 39, 1010428317713390.
5. Fan, X.; Wen, L.; Li, Y.; Lou, L.; Liu, W.; Zhang, J. The expression profile and prognostic value of APE/Ref-1 and NPM1 in high-grade serous ovarian adenocarcinoma. *APMIS* **2017,** 125, 857-862.
6. Li, M.; Wilson, D. M., 3rd. Human apurinic/apyrimidinic endonuclease 1. *Antioxid Redox Signal* **2014,** 20, 678-707.
7. Madhusudan, S.; Smart, F.; Shrimpton, P.; Parsons, J. L.; Gardiner, L.; Houlbrook, S.; Talbot, D. C.; Hammonds, T.; Freemont, P. A.; Sternberg, M. J.; Dianov, G. L.; Hickson, I. D. Isolation of a small molecule inhibitor of DNA base excision repair. *Nucleic Acids Res* **2005,** 33, 4711-4724.
8. Seiple, L. A.; Cardellina, J. H., 2nd; Akee, R.; Stivers, J. T. Potent inhibition of human apurinic/apyrimidinic endonuclease 1 by arylstibonic acids. *Mol Pharmacol* **2008,** 73, 669-677.
9. Zawahir, Z.; Dayam, R.; Deng, J.; Pereira, C.; Neamati, N. Pharmacophore guided discovery of small-molecule human apurinic/apyrimidinic endonuclease 1 inhibitors. *J Med Chem* **2009,** 52, 20-32.
10. Bapat, A.; Glass, L. S.; Luo, M.; Fishel, M. L.; Long, E. C.; Georgiadis, M. M.; Kelley, M. R. Novel small molecule inhibitor of Ape1 endonuclease blocks proliferation and reduces viability of glioblastoma cells. *J Pharmacol Exp Ther.* **2010,** 334, 988-998.
11. Simeonov, A.; Kulkarni, A.; Dorjsuren, D.; Jadhav, A.; Shen, M.; McNeill, D. R.; Austin, C. P.; Wilson, D. M., 3rd. Identification and characterization of inhibitors of human apurinic/apyrimidinic endonuclease APE1. *PLoS One* **2009,** 4, e5740.
12. Mohammed, M. Z.; Vyjayanti, V. N.; Laughton, C. A.; Dekker, L. V.; Fischer, P. M.; Wilson, D. M., 3rd; Abbotts, R.; Shah, S.; Patel, P. M.; Hickson, I. D.; Madhusudan, S. Development and evaluation of human AP endonuclease inhibitors in melanoma and glioma cell lines. *Br J Cancer* **2011,** 104, 653-663.
13. Kaur, G.; Cholia, R. P.; Mantha, A. K.; Kumar, R. DNA repair and redox activities and inhibitors of apurinic/apyrimidinic endonuclease 1/redox effector factor 1 (APE1/Ref-1): a comparative analysis and their scope and limitations toward anticancer drug development. *J Med Chem* **2014,** 57, 10241-10256.
14. Kotera, N.; Poyer, F.; Granzhan, A.; Teulade-Fichou, M. P. Efficient inhibition of human AP endonuclease 1 (APE1) via substrate masking by abasic site-binding macrocyclic ligands. *Chem Commun (Camb)* **2015,** 51, 15948-15951.

15. Wilson, D. M., 3rd; Simeonov, A. Small molecule inhibitors of DNA repair nuclease activities of APE1. *Cell Mol Life Sci* **2010,** 67, 3621-3631.
16. Rai, G.; Vyjayanti, V. N.; Dorjsuren, D.; Simeonov, A.; Jadhav, A.; Wilson, D. M., 3rd; Maloney, D. J. Synthesis, biological evaluation, and structure-activity relationships of a novel class of apurinic/apyrimidinic endonuclease 1 inhibitors. *J Med Chem* **2012,** 55, 3101-3112.
17. Ogbourne, S. M.; Parsons, P. G. The value of nature's natural product library for the discovery of New Chemical Entities: the discovery of ingenol mebutate. *Fitoterapia* **2014,** 98, 36-44.
18. Wessjohann, L. A.; Ruijter, E.; Garcia-Rivera, D.; Brandt, W. What can a chemist learn from nature's macrocycles?--a brief, conceptual view. *Mol Divers* **2005,** 9, 171-186.
19. Lipinski, C. A. Lead- and drug-like compounds: the rule-of-five revolution. *Drug Discov Today Technol* **2004,** 1, 337-341.
20. Lipinski, C. A. Rule of five in 2015 and beyond: Target and ligand structural limitations, ligand chemistry structure and drug discovery project decisions. *Adv Drug Deliv Rev* **2016,** 101, 34-41.
21. Villar, E. A.; Beglov, D.; Chennamadhavuni, S.; Porco, J. A., Jr.; Kozakov, D.; Vajda, S.; Whitty, A. How proteins bind macrocycles. *Nat Chem Biol* **2014,** 10, 723-731.
22. Giordanetto, F.; Kihlberg, J. Macrocyclic drugs and clinical candidates: what can medicinal chemists learn from their properties? *J Med Chem* **2014,** 57, 278-295.
23. Driggers, E. M.; Hale, S. P.; Lee, J.; Terrett, N. K. The exploration of macrocycles for drug discovery--an underexploited structural class. *Nat Rev Drug Discov* **2008,** 7, 608-624.
24. Yu, X.; Sun, D. Macrocyclic drugs and synthetic methodologies toward macrocycles. *Molecules* **2013,** 18, 6230-6268.
25. Heinis, C. Drug discovery: tools and rules for macrocycles. *Nat Chem Biol* **2014,** 10, 696-698.
26. Marsault, E.; Peterson, M. L. Macrocycles are great cycles: applications, opportunities, and challenges of synthetic macrocycles in drug discovery. *J Med Chem* **2011,** 54, 1961-2004.
27. Mol, C. D.; Izumi, T.; Mitra, S.; Tainer, J. A. DNA-bound structure and mutants reveal abasic DNA binding by APE1 DNA repair and coordination. *Nature* **2000,** 403, 451-456.
28. He, H.; Chen, Q.; Georgiadis, M. M. High-resolution crystal structures reveal plasticity in the metal binding site of apurinic/apyrimidinic endonuclease I. *Biochemistry* **2014,** 53, 6520-6529.
29. Wu, J.; Zhu, K. C.; Yuan, P. W.; Panek, J. S. Bifunctional homoallylic carbamates from chiral silane additions to in situ generated N-acyl iminium ions. *Org Lett* **2012,** 14, 3624-3627.
30. Beresis, R. T.; Solomon, J. S.; Yang, M. G.; Jain, N. F.; Panek, J. S. Synthesis of chiral (E)-Cryotylsilanes: [3R- and 3S-]-(4E)-Methyl e-(Dimethylphenylsilyl)-4-Hexenoate. *Org Synth* **1998**, 75, 78.
31. Beeler, A. B.; Acquilano, D. E.; Su, Q.; Yan, F.; Roth, B. L.; Panek, J. S.; Porco, J. A., Jr. Synthesis of a library of complex macrodiolides employing cyclodimerization of hydroxy esters. *J Comb Chem* **2005,** 7, 673-681.
32. Nakajima, Y. Mechanisms of bacterial resistance to macrolide antibiotics. *J Infect Chemother* **1999,** 5, 61-74.
33. Morar, M.; Pengelly, K.; Koteva, K.; Wright, G. D. Mechanism and diversity of the erythromycin esterase family of enzymes. *Biochemistry* **2012,** 51, 1740-1751.
34. Fishel, M. L.; He, Y.; Reed, A. M.; Chin-Sinex, H.; Hutchins, G. D.; Mendonca, M. S.; Kelley, M. R. Knockdown of the DNA repair and redox signaling protein Ape1/Ref-1 blocks ovarian cancer cell and tumor growth. *DNA Repair (Amst)* **2008,** 7, 177-186.
35. Collins, A. R. The comet assay for DNA damage and repair: principles, applications, and limitations. *Mol Biotechnol* **2004,** 26, 249-261.
36. Hartmann, A.; Agurell, E.; Beevers, C.; Brendler-Schwaab, S.; Burlinson, B.; Clay, P.; Collins, A.; Smith, A.; Speit, G.; Thybaud, V.; Tice, R. R.; th International Comet Assay, W. Recommendations for conducting the in vivo alkaline Comet assay. 4th International Comet Assay Workshop. *Mutagenesis* **2003,** 18, 45-51.
37. Georgiadis, M.; Luo, M.; Gaur, R.; Delaplane, S.; Li, X.; Kelley, M. Evolution of the redox function in mammalian apurinic/apyrimidinic endonuclease. *Mutat Res* **2008,** 643, 54-63.

38. Otwinowski, Z.; Minor, W. Processing of X-ray diffraction data collected in oscillation mode. *Methods Enzymol* **1997,** 276, 307-326.
39. Bruker. SAINT, SADABS & XPREP. *Bruker AXS Inc.* **2007**, Madison, Wisconsin, USA.
40. Brenke, R.; Kozakov, D.; Chuang, G. Y.; Beglov, D.; Hall, D.; Landon, M. R.; Mattos, C.; Vajda, S. Fragment-based identification of druggable 'hot spots' of proteins using Fourier domain correlation techniques. *Bioinformatics* **2009,** 25, 621-627.
41. Kozakov, D.; Grove, L. E.; Hall, D. R.; Bohnuud, T.; Mottarella, S. E.; Luo, L.; Xia, B.; Beglov, D.; Vajda, S. The FTMap family of web servers for determining and characterizing ligand-binding hot spots of proteins. *Nat Protoc* **2015,** 10, 733-755.
42. Ngan, C. H.; Hall, D. R.; Zerbe, B.; Grove, L. E.; Kozakov, D.; Vajda, S. FTSite: high accuracy detection of ligand binding sites on unbound protein structures. *Bioinformatics* **2012,** 28, 286-7.
43. Morris, G. M.; Huey, R.; Lindstrom, W.; Sanner, M. F.; Belew, R. K.; Goodsell, D. S.; Olson, A. J. AutoDock4 and AutoDockTools4: Automated docking with selective receptor flexibility. *J Comput Chem* **2009,** 30, 2785-2791.
44. *Marvin 6.1.0, ChemAxon* http://www.chemaxon.com, 2013.
45. Bapat, A.; Glass, L. S.; Luo, M.; Fishel, M. L.; Long, E. C.; Georgiadis, M. M.; Kelley, M. R. Novel small-molecule inhibitor of apurinic/apyrimidinic endonuclease 1 blocks proliferation and reduces viability of glioblastoma cells. *J Pharmacol Exp Ther* **2010,** 334, 988-998.
46. Logsdon, D. P.; Grimard, M.; Luo, M.; Shahda, S.; Jiang, Y.; Tong, Y.; Yu, Z.; Zyromski, N.; Schipani, E.; Carta, F.; Supuran, C. T.; Korc, M.; Ivan, M.; Kelley, M. R.; Fishel, M. L. Regulation of HIF1alpha under hypoxia by APE1/Ref-1 impacts CA9 expression: Dual targeting in patient-derived 3D pancreatic cancer models. *Mol Cancer Ther* **2016,** 15, 2722-2732.
47. Logsdon, D. P.; Cheng, H.; Luo, M.; Shahda, S.; Ivan, M.; Hao, Y.; Tong, Y.; Yu, Z.; Zyromski, N.; Schipani, E.; Liu, Y.; Supuran, C. T.; Kelley, M. R.; Fishel, M. L. Targeting APE1/Ref-1 results in inhibition of hypoxia signaling genes. In *AACR-NC-EORTC International Conference: Molecular Targets and Cancer Therapeutics*, Mol Cancer Ther December 2015 14; B158: Boston, MA, 2015.

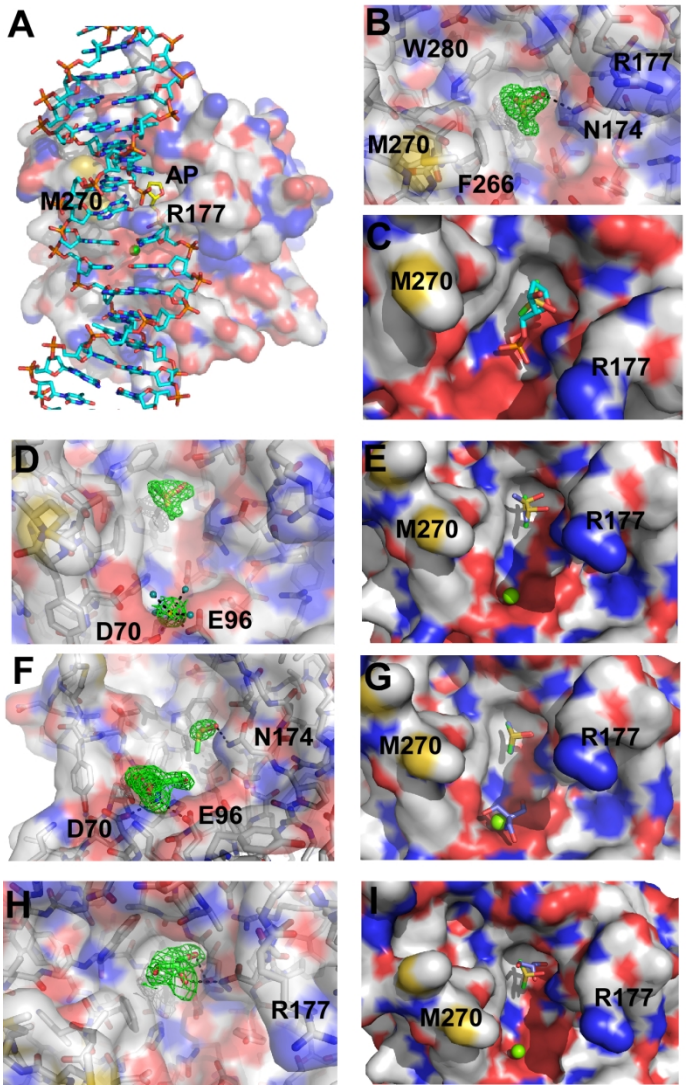

Figure 1.

168x182mm (300 x 300 DPI)

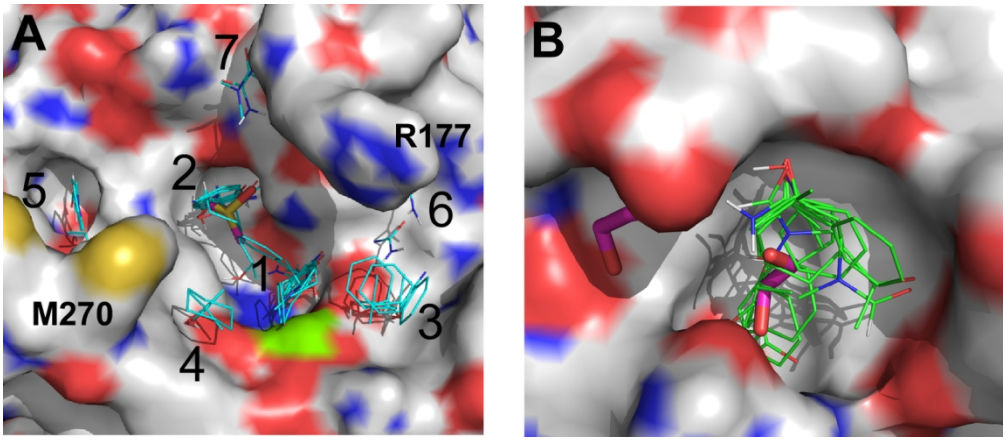

Figure 2.

129x55mm (300 x 300 DPI)

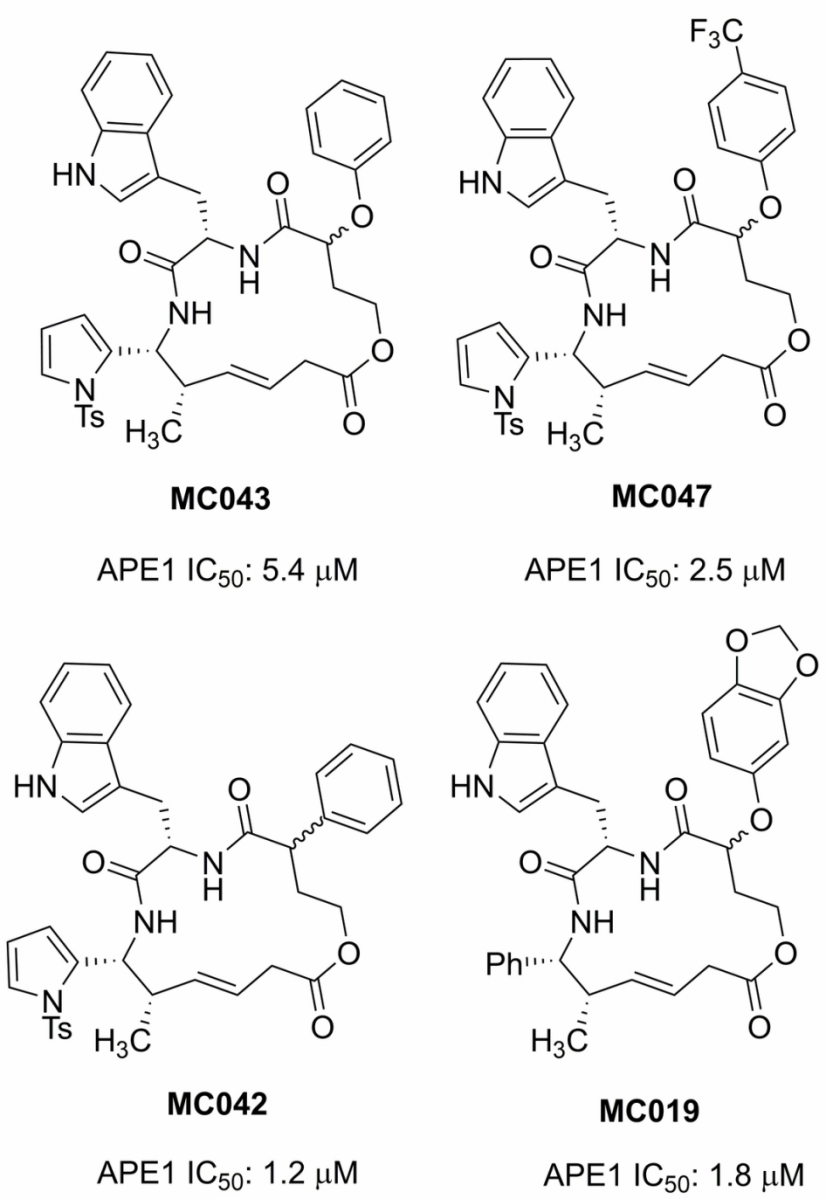

Figure 3.

92x134mm (300 x 300 DPI)

Figure 4.

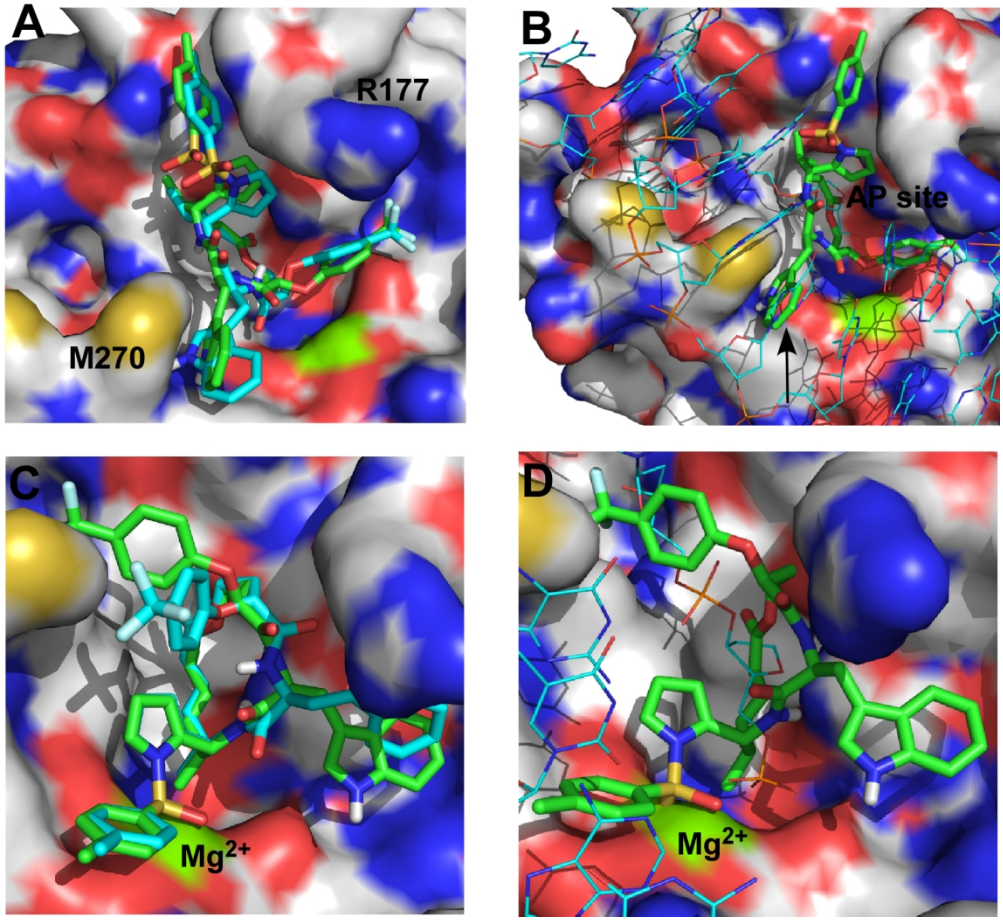

Figure 4.

136x135mm (300 x 300 DPI)

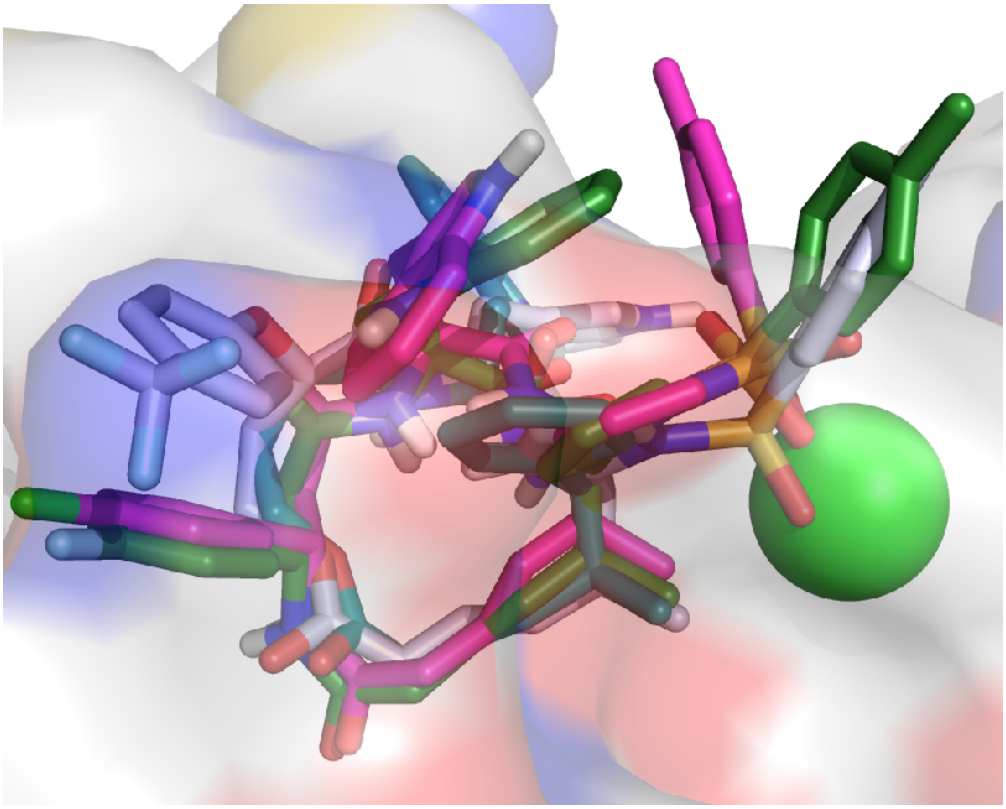

Figure 5.

68x54mm (300 x 300 DPI)

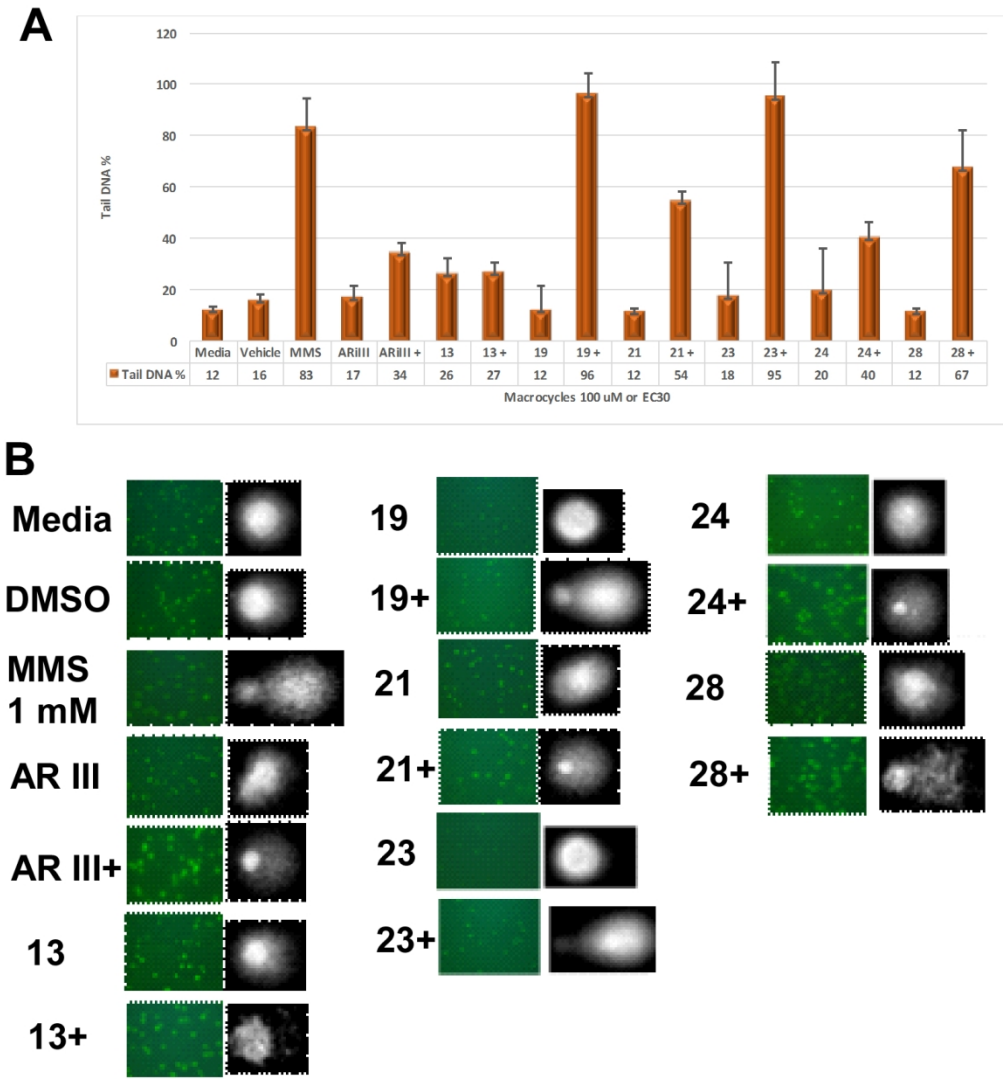

Figure 6.

138x149mm (300 x 300 DPI)

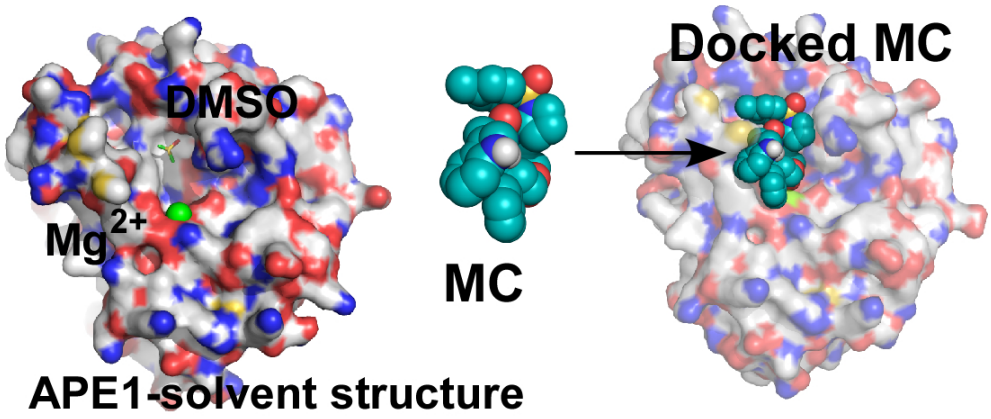

94x39mm (300 x 300 DPI)